Chapter 6

EXTERNAL PHOTON BEAMS: PHYSICAL ASPECTS

E.B. PODGORSAK
Department of Medical Physics,
McGill University Health Centre,
Montreal, Quebec, Canada

6.1. INTRODUCTION

Radiotherapy procedures fall into two main categories: external beam radiotherapy and brachytherapy. In external beam radiotherapy the radiation source is at a certain distance from the patient and the target within the patient is irradiated with an external radiation beam. In brachytherapy (see Chapter 13) radiation sources are placed directly into the target volume (intracavitary or interstitial brachytherapy) or on to a target (surface mould or intraoperative radiotherapy). Most external beam radiotherapy is carried out with photon beams, some with electron beams and a very small fraction with more exotic particles such as protons, heavier ions or neutrons.

This chapter deals with external photon beam radiotherapy. Photon external beams are all characterized by the same physical parameters, but fall into various categories depending on their origin, means of production and energy. There are two origins of photon beams: γ rays, which originate from radioactive nuclei, and X rays, which originate in a target bombarded with energetic electrons. The X rays from a target consist of bremsstrahlung photons and characteristic photons. X rays are produced either in an X ray tube (superficial or orthovoltage X rays) or in a linac (megavoltage X rays).

6.2. QUANTITIES USED IN DESCRIBING A PHOTON BEAM

Radiation dosimetry deals with two distinctly different entities: one describes the photon radiation beam itself in terms of the number and energies of photons constituting the photon beam and the other describes the amount of energy the photon beam may deposit in a given medium such as air, water or biological material.

6.2.1. Photon fluence and photon fluence rate

The photon fluence ϕ is defined as the quotient dN by dA, where dN is the number of photons that enter an imaginary sphere of cross-sectional area dA:

$$\phi = \frac{\mathrm{d}N}{\mathrm{d}A} \tag{6.1}$$

The unit of photon fluence ϕ is cm^{-2}.
The photon fluence rate is defined as the photon fluence per unit time:

$$\varphi = \frac{\mathrm{d}\phi}{\mathrm{d}t} \tag{6.2}$$

The unit of photon fluence rate is $cm^{-2} \cdot s^{-1}$.

6.2.2. Energy fluence and energy fluence rate

The energy fluence Ψ describes the energy flow in a photon beam and is defined as the amount of energy dE crossing a unit area dA:

$$\Psi = \frac{\mathrm{d}E}{\mathrm{d}A} \tag{6.3}$$

The unit of energy fluence Ψ is MeV/cm^2.

For a monoenergetic beam, dE is the number of photons dN times their energy $h\nu$, and the energy fluence Ψ in terms of photon fluence ϕ is:

$$\Psi = \phi h\nu \tag{6.4}$$

The energy fluence rate Ψ is defined as the energy fluence per unit time:

$$\Psi = \frac{\mathrm{d}\psi}{\mathrm{d}t} \tag{6.5}$$

The unit of energy fluence rate is $MeV \cdot cm^{-2} \cdot s^{-1}$.

6.2.3. Air kerma in air

For a monoenergetic photon beam in air the air kerma in air $(K_{air})_{air}$ at a given point away from the source is proportional to the energy fluence Ψ or photon fluence ϕ as follows:

$$(K_{air})_{air} = \psi \left(\frac{\mu_{tr}}{\rho}\right)_{air} = \phi h\nu \left(\frac{\mu_{tr}}{\rho}\right)_{air} \tag{6.6}$$

where $(\mu_{tr}/\rho)_{air}$ is the mass–energy transfer coefficient for air at photon energy $h\nu$.

Kerma K consists of two components: the collision kerma K^{col} and the radiative kerma K^{rad}:

$$K = K^{col} + K^{rad} \tag{6.7}$$

For monoenergetic photons in air the collision kerma K^{col} is proportional to Ψ and ϕ through the following relationship:

$$K^{col} = \psi \left(\frac{\mu_{ab}}{\rho}\right)_{air} = h\nu\phi \left(\frac{\mu_{ab}}{\rho}\right)_{air} \tag{6.8}$$

where $(\mu_{ab}/\rho)_{air}$ is the mass–energy absorption coefficient for air at photon energy $h\nu$. Often in the literature the energy absorption coefficient μ_{ab} is denoted as μ_{en}.

The mass–energy transfer coefficient (μ_{tr}/ρ) and mass–energy absorption coefficient (μ_{ab}/ρ) are related through the following relationship:

$$\frac{\mu_{ab}}{\rho} = \frac{\mu_{tr}}{\rho}(1 - \bar{g}) \tag{6.9}$$

where $\bar{g}$ is the radiative fraction (i.e. the fraction of the energy of secondary charged particles (electrons) that is lost to bremsstrahlung rather than being deposited in the medium). For low atomic number Z materials and photon energies below 1 MeV, the radiative fraction $\bar{g} \approx 0$, $(\mu_{tr}/\rho) \approx (\mu_{ab}/\rho)$ and $K \approx K^{col}$.

6.2.4. Exposure in air

The collision air kerma in air $(K_{\text{air}}^{\text{col}})_{\text{air}}$ is related to exposure in air X through the following relationship:

$$(K_{\text{air}}^{\text{col}})_{\text{air}} = X(W_{\text{air}}/e) \tag{6.10}$$

where (W_{air}/e), as discussed in Section 9.1.3, is the average energy required to produce an ion pair in dry air (33.97 eV/ion pair).

The special unit of exposure is the roentgen (R), while the SI unit is 2.58×10^{-4} C/kg with 1 R = 2.58×10^{-4} C/kg. Thus:

$$(K_{\text{air}}^{\text{col}})_{\text{air}} = \left(2.58 \times 10^{-4} \frac{\text{C}}{\text{kg}_{\text{air}}\text{R}}\ 33.97 \frac{\text{J}}{\text{C}}\right) X = \left(0.876 \frac{\text{cGy}}{\text{R}}\right) X \tag{6.11}$$

with the exposure X given in roentgens.

6.2.5. Dose to small mass of medium in air

The concept 'dose to small mass of medium in air', also known as 'dose in free space', was introduced by Johns and Cunningham to characterize the output of a radiation unit and to gain a reference dose for dosimetric calculations involving tissue–air ratios (TARs) and peak scatter factors (PSFs). The 'dose to small mass of medium in air' is designated as D'_{med} and is based on a measurement of the air kerma in air. The concept has gained widespread use in orthovoltage and ^{60}Co therapy, but is of limited use in megavoltage linac beam therapy.

The steps involved in determining the 'dose to small mass of medium in air' D'_{med} at point P in a radiation beam from a signal M_{P} measured with an ionization chamber centred at point P in air are:

$$M_{\text{P}} \overset{(1)}{\rightarrow} X_{\text{P}} \overset{(2)}{\rightarrow} (K_{\text{air}})_{\text{air}} \overset{(3)}{\rightarrow} (K_{\Delta m})_{\text{air}} \overset{(4)}{\rightarrow} (K_{\text{med}})_{\text{air}} \overset{(5)}{\rightarrow} D'_{\text{med}} \tag{6.12}$$

where M_{P} is the signal measured with an ionization chamber at point P and corrected for influence quantities such as air temperature, air pressure and recombination loss (see Section 9.3). The ionization chamber should have an

appropriate buildup cap and an exposure calibration coefficient in air N_X or an air kerma in air calibration coefficient N_K.

- Step 1: Determine X_P, the exposure at point P, through:

$$X_P = M_P N_X \tag{6.13}$$

- Step 2: Determine $(K_{air})_{air}$, the air kerma in air at point P, through:

$$(K_{air})_{air} = 0.876 \frac{\text{cGy}}{\text{R}} X_P \tag{6.14}$$

Alternatively, $(K_{air})_{air}$ may be determined from M_P directly, if N_K for the chamber is known, as follows:

$$(K_{air})_{air} = M_P N_K \tag{6.15}$$

- Step 3: Determine collision kerma to Δm, an infinitesimal mass of any other material (e.g. water), in air from:

$$(K_{\Delta m})_{air} = (K_{air})_{air} \left(\frac{\bar{\mu}_{ab}}{\rho} \right)_{air}^{\Delta m} \tag{6.16}$$

where $(\bar{\mu}_{ab}/\rho)_{air}^{\Delta m}$ is the ratio of spectrum averaged mass–energy absorption coefficients for Δm and air.

- Step 4: Determine collision kerma to a spherical mass of medium centred around P and having a radius r_{med} just large enough to provide charged particle equilibrium (CPE) at point P:

$$(K_{med})_{air} = (K_{\Delta m})_{air}(r_{med}) \tag{6.17}$$

where $k(r_{med})$ is a correction factor accounting for the photon beam attenuation in the spherical mass of medium and approximated as:

$$k(r_{med}) \approx e^{-\left(\frac{\mu_{ab}}{\rho}\right)_{med} \rho r_{med}} \tag{6.18}$$

$(\mu_{ab}/\rho)_{med}$ in Eq. (6.18) is the mass–energy absorption coefficient and ρ is the density of the medium. For water, which is usually chosen as the

medium, $k(r_{med}) \approx 0.985$ for ^{60}Co photons and approximately 1 for lower photon energies.

- Step 5: 'Dose to small mass of medium in free space' D'_{med} is obtained from the following relationship:

$$D'_{med} = \beta(K_{med})_{air} = \beta 0.876 \frac{\text{cGy}}{\text{R}} \left(\frac{\mu_{ab}}{\rho}\right)^{med}_{air} X_P k(r_{med}) \quad (6.19)$$

where β is a proportionality constant equal to 1.003, 1.001 and 1.0 for ^{60}Co, ^{137}Cs and X rays below 350 kVp, respectively. Often β is assumed equal to 1, even for ^{60}Co γ rays.

The product:

$$0.876 \frac{\text{cGy}}{\text{R}} \left(\frac{\mu_{ab}}{\rho}\right)^{med}_{air}$$

is usually referred to as the roentgen to cGy conversion factor $f_{med,}$ and the 'dose to small mass of medium in air', assuming that $\beta \approx 1$, can then be written as:

$$D'_{med} = f_{med} Xk(\text{r}_{med}) \quad (6.20)$$

6.3. PHOTON BEAM SOURCES

Photon sources are either isotropic or non-isotropic and they emit either monoenergetic or heterogeneous photon beams. The most common photon sources used in radiation oncology are X ray machines, teletherapy radio-isotope sources and linacs.

- An isotropic photon source produces the same photon fluence rate in all directions, while the photon fluence rate from a non-isotropic source depends on the direction of measurement.
- A plot of number of photons per energy interval versus photon energy is referred to as a photon spectrum. Photon spectra for a monoenergetic and a heterogeneous photon beam are shown in Figs 6.1(a) and (b), respectively. The area under the curve in Fig. 6.1(b) represents the total number of photons in the beam:

$$\phi = \int \frac{\mathrm{d}\phi(h\nu)}{\mathrm{d}h\nu}\,\mathrm{d}h\nu \tag{6.21}$$

- All photons in a monoenergetic photon beam have the same energy $h\nu$ (Fig. 6.1(a)). Photons in a heterogeneous X ray beam form a distinct spectrum, with photons present in all energy intervals from 0 to a maximum value $h\nu_{max}$, which is equal to the kinetic energy of electrons striking the target (Fig. 6.1(b)).
- In Fig. 6.1(b) the two spikes in the spectrum represent characteristic photons, while the continuous spectrum from 0 to $h\nu_{max}$ represents bremsstrahlung photons.
- γ ray sources are usually isotropic and produce monoenergetic photon beams, while X ray targets are non-isotropic sources producing heterogeneous photon spectra.
- Narrow monoenergetic photon beams will have identical first and second half-value layers (HVLs). In narrow heterogeneous photon beams, on the other hand, the second HVL will be either larger or smaller than the first HVL: larger in the superficial and orthovoltage range because of beam hardening effects and smaller in the high megavoltage range because of beam softening effects.

6.4. INVERSE SQUARE LAW

In external beam radiotherapy, photon sources are often assumed to be point sources and the beams they produce are divergent beams, as shown schematically in Fig. 6.2. Let us assume that we have a photon point source S and a square field with side a (area $A = a^2$) at a distance f_a from the source. At

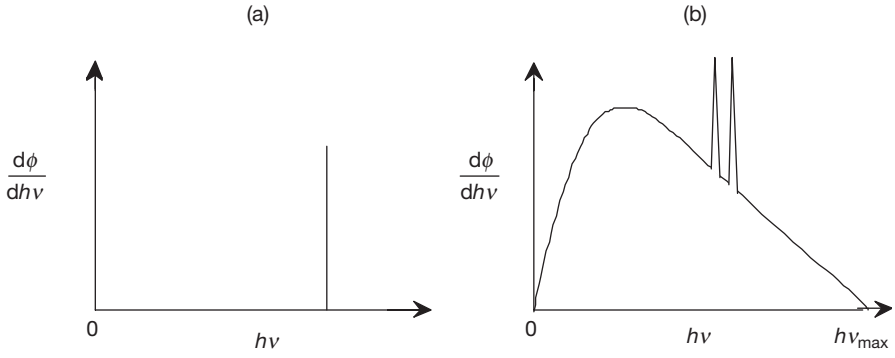

FIG. 6.1. Typical spectra for (a) monoenergetic and (b) heterogeneous photon beams.

a distance f_b we then have a square field with side b (area $B = b^2$), and the two fields are geometrically related as follows:

$$tg\beta = \frac{a/2}{f_a} = \frac{b/2}{f_b}$$

or (6.22)

$$\frac{a}{b} = \frac{f_a}{f_b}$$

where β is the angle between the beam central axis and the geometric beam edge.

The photon source S emits photons and produces a photon fluence ϕ_A at distance f_a and a photon fluence ϕ_B at distance f_b. Since the total number of

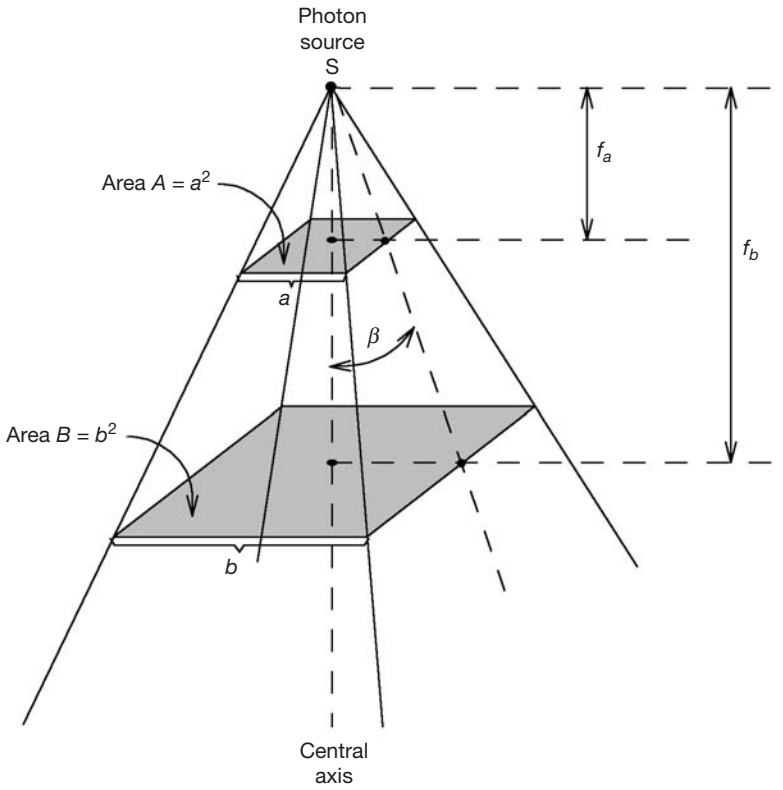

FIG. 6.2. Divergent photon beam originating in a photon point source. At distance f_a from the source S the field size is $A = a^2$, at distance f_b the field size is $B = b^2$.

photons N_{tot} crossing area A is equal to the total number of photons crossing area B (assuming no photon interactions take place in air between area A and area B), we can write:

$$N_{tot} = \phi_A A = \phi_B B$$

and

$$\frac{\phi_A}{\phi_B} = \frac{B}{A} = \frac{b^2}{a^2} = \frac{f_b^2}{f_a^2} \tag{6.23}$$

The photon fluence is thus inversely proportional to the square of the distance from the source. For example, if $f_b = 2f_a$ then the photon fluence at B will be exactly 1/4 of the photon fluence at A (i.e. $\phi_B = \phi_A/4$).

Since at a given point P in air the exposure in air X, air kerma in air $(K_{air})_{air}$ and 'dose to small mass of medium in air' D'_{med} are directly proportional to the photon fluence at point P, it is reasonable to conclude that the three quantities X, $(K_{air})_{air}$ and D'_{med} all follow this inverse square law behaviour:

$$\frac{X(f_a)}{X(f_b)} = \frac{(K_{air}(f_a))_{air}}{(K_{air}(f_b))_{air}} = \frac{D'_{med}(f_a)}{D'_{med}(f_b)} = \left(\frac{f_b}{f_a}\right)^2 \tag{6.24}$$

6.5. PENETRATION OF PHOTON BEAMS INTO A PHANTOM OR PATIENT

A photon beam propagating through air or a vacuum is governed by the inverse square law; a photon beam propagating through a phantom or patient, on the other hand, is affected not only by the inverse square law but also by the attenuation and scattering of the photon beam inside the phantom or patient. These three effects make the dose deposition in a phantom or patient a complicated process and its determination a complex task.

A direct measurement of the dose distribution inside the patient is essentially impossible, yet for a successful outcome of patient radiation treatment it is imperative that the dose distribution in the irradiated volume be known precisely and accurately. This is usually achieved through the use of several functions that link the dose at any arbitrary point inside the patient to the known dose at the beam calibration (or reference) point in a phantom.

The functions are usually measured with suitable radiation detectors in tissue equivalent phantoms, and the dose or dose rate at the reference point is determined for, or in, water phantoms for a specific set of reference conditions, such as depth, field size and source to surface distance (SSD), as discussed in detail in Section 9.1.

A typical dose distribution on the central axis of a megavoltage photon beam striking a patient is shown in Fig. 6.3. Several important points and regions may be identified. The beam enters the patient on the surface, where it delivers a certain surface dose D_s. Beneath the surface the dose first rises rapidly, reaches a maximum value at depth z_{max} and then decreases almost exponentially until it reaches a value D_{ex} at the patient's exit point. The techniques for relative dose measurements are discussed in detail in Section 6.13.

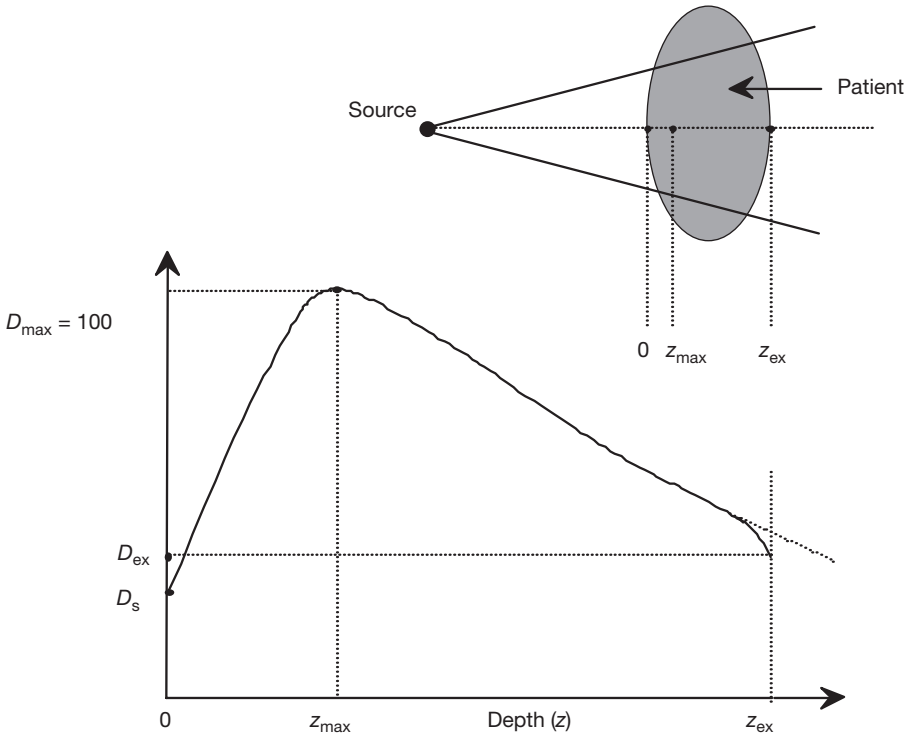

FIG. 6.3. Dose deposition from a megavoltage photon beam in a patient. D_s is the surface dose at the beam entrance side, D_{ex} is the surface dose at the beam exit side. D_{max} is the dose maximum often normalized to 100, resulting in a depth dose curve referred to as the percentage depth dose (PDD) distribution. The region between $z = 0$ and $z = z_{max}$ is referred to as the dose buildup region.

6.5.1. Surface dose

For megavoltage photon beams the surface dose is generally much lower than the maximum dose, which occurs at a depth z_{max} beneath the patient's surface. In megavoltage photon beams the surface dose depends on the beam energy and field size.

The larger the photon beam energy, the lower the surface dose, which for a 10×10 cm^2 field typically amounts to some 30% of the maximum dose for a cobalt beam, 15% for a 6 MV X ray beam and 10% for an 18 MV X ray beam. For a given beam energy the surface dose increases with the field size.

The low surface dose compared with the maximum dose is referred to as the skin sparing effect and represents an important advantage of megavoltage beams over orthovoltage and superficial beams in the treatment of deep seated tumours.

Orthovoltage and superficial beams do not exhibit the skin sparing effect, since their dose maximum occurs on the skin surface (i.e. the surface dose is equal to the maximum dose).

The surface dose is measured with thin window parallel-plate ionization chambers for both chamber polarities, with the average reading between the positive and negative polarities taken as the surface dose value (see Section 6.13).

The surface dose represents contributions to the dose from:

- Photons scattered from the collimators, flattening filter and air;
- Photons backscattered from the patient;
- High energy electrons produced by photon interactions in air and any shielding structures in the vicinity of the patient.

6.5.2. Buildup region

The dose region between the surface (depth $z = 0$) and depth $z = z_{max}$ in megavoltage photon beams is referred to as the dose buildup region and results from the relatively long range of energetic secondary charged particles (electrons and positrons) that first are released in the patient by photon interactions (photoelectric effect, Compton effect, pair production) and then deposit their kinetic energy in the patient (see Section 2.7.3).

- In the region immediately beneath the patient's surface, the condition of CPE does not exist and the absorbed dose is much smaller than the collision kerma. However, as the depth z increases, CPE is eventually reached at $z = z_{max}$, where z is approximately equal to the range of

secondary charged particles and the dose becomes comparable with the collision kerma.

- Beyond z_{max} both the dose and collision kerma decrease because of the photon attenuation in the patient, resulting in a transient rather than true CPE.

6.5.3. Depth of dose maximum z_{max}

The depth of dose maximum z_{max} beneath the patient's surface depends on the beam energy and beam field size. The beam energy dependence is the main effect; the field size dependence is often ignored because it represents only a minor effect.

Nominal values for z_{max} range from zero for superficial and orthovoltage X ray beams, through 0.5 cm for ^{60}Co beams, to 5 cm for 25 MV beams, as shown in Table 6.1.

For a given beam energy, the largest z_{max} occurs for fields of ~5 × 5 cm^2. For fields larger than 5 × 5 cm^2, z_{max} decreases because of collimator scatter effects (for cobalt units) and collimator and flattening filter scatter effects (for linacs). For fields smaller than 5 × 5 cm^2, z_{max} decreases because of phantom scatter effects.

6.5.4. Exit dose

The dose delivered to the patient at the beam exit point is referred to as the exit dose. As shown schematically in Fig. 6.3, close to the beam exit point the dose distribution curves slightly downwards from the extrapolated dose distribution curve. This relatively small effect is attributed to the missing scatter contribution at the exit point from points beyond the exit dose point. Similarly to the surface dose, the exit dose may be measured with a parallel-plate chamber, in this case with the chamber body orientated towards the source.

6.6. RADIATION TREATMENT PARAMETERS

External beam radiotherapy with photon beams is carried out with three types of treatment machine: X ray units, isotope teletherapy units (mainly ^{60}Co units) and linacs. The main parameters in external beam dose delivery with photon beams are the: (a) depth of treatment; (b) field size; (c) SSD in SSD set-ups or source to axis distance (SAD) in SAD (isocentric) set-ups; and (d) photon beam energy.

TABLE 6.1. TYPICAL DEPTHS OF DOSE MAXIMUM z_{max} FOR VARIOUS PHOTON BEAM ENERGIES AND A FIELD SIZE OF 5×5 cm^2

	Superficial	Orthovoltage	Co-60	4 MV	6 MV	10 MV	18 MV	25 MV
z_{max} (cm)	0	0	0.5	1	1.5	2.5	3.5	5

6.6.1. Radiation beam field size

Beams used for radiotherapy have various shapes that usually represent a compromise between the actual target shape and the need for simplicity and efficiency in beam shaping. Four general groups of field shape are used in radiotherapy: square, rectangular, circular and irregular.

Square and rectangular fields are usually produced with collimators installed in radiotherapy machines, circular fields with special collimators attached to the treatment machine and irregular fields with custom made shielding blocks or with multileaf collimators (MLCs) attached to the treatment machine.

For any arbitrary radiation field an equivalent square or circular field may be found, meaning that the arbitrary field and the equivalent square or circular field will be characterized with similar beam parameters and functions that are of importance in radiation dosimetry.

An arbitrary rectangular field with sides a and b will be approximately equivalent to a square radiation field with sides a_{eq} when both fields have the same area/perimeter ratio (Day's rule):

$$\frac{ab}{2(a+b)} = \frac{a_{eq}{}^2}{4a_{eq}}$$

or

$$a_{eq} = \frac{2ab}{a+b} \tag{6.25}$$

An arbitrary square field with sides a_{eq} will be equivalent to a circular field with radius r_{eq} when both fields have the same area:

$$a_{eq}^2 = \pi r_{eq}^2$$

or

$$r_{eq} = \frac{a_{eq}}{\sqrt{\pi}} \tag{6.26}$$

6.6.2. Collimator factor

Exposure in air, air kerma in air and 'dose to small mass of medium in air' at a given point P in air contain contributions from two components: primary and scatter.

- The primary component is the major component; it comes directly from the source and does not depend on the field size.
- Scatter represents a minor yet non-negligible component; it consists of photons scattered into point P mainly from the collimator but also possibly from the air and the flattening filter of a linac. The scatter component depends on field size A (collimator setting): the larger the field size, the larger the collimator surface available for scattering and consequently the larger the scatter component.

Exposure in air X, air kerma in air $(K_{air})_{air}$ and 'dose to small mass of medium in air' D'_{med} depend on field size A and a parameter referred to as the collimator factor (CF) (or collimator scatter factor S_c in Khan's notation, or relative exposure factor (REF) in 1970s notation). The CF is defined as:

$$\mathrm{CF}(A,h\nu) = S_c(A,h\nu) = \mathrm{REF}(A,h\nu)$$

$$= \frac{X(A,h\nu)}{X(10,h\nu)} = \frac{(K_{air}(A,h\nu))_{air}}{(K_{air}(10,h\nu))_{air}} = \frac{D'(A,h\nu)}{D'(10,h\nu)} \tag{6.27}$$

The geometry for the measurement of the CF is shown in Fig. 6.4; Fig. 6.4(a) shows the measurement of $D'(A, h\nu)$, while Fig. 6.4(b) shows the measurement of $D'(10, h\nu)$.

The CF is usually measured with an ionization chamber with a buildup cap of a size large enough to provide maximum dose buildup for the given energy beam. For small fields one may carry out the measurements at large distances from the source so that the buildup cap is fully covered; however, the data are usually corrected back to the nominal SSD of the machine by using the inverse square law.

The CF is normalized to 1 for the nominal field of 10×10 cm^2 at the nominal SSD for the treatment machine. It is larger than 1 for fields A exceeding 10×10 cm^2 and smaller than 1 for fields A smaller than 10×10 cm^2. It is usually measured at point P in air with a cylindrical ionization chamber equipped with an appropriate buildup cap and the chamber centre placed at (nominal SSD + z_{max}) from the source. SSD here stands for the nominal SSD

(typically 80 or 100 cm for cobalt units and 100 cm for linacs) and z_{max} for the depth of dose maximum in a phantom for the specific photon beam.

In some centres the CF is measured at the machine isocentre. The results are essentially identical to those obtained with measurements carried out at point P in air.

6.6.3. Peak scatter factor

The 'dose to small mass of medium' D'_P is measured with just enough material around the point of interest P to provide electronic equilibrium (ionization chamber with appropriate buildup cap). D'_P is related to D_P, the dose at z_{max} in a phantom at point P, through the PSF as follows:

$$\mathrm{PSF}(A,h\nu) = \frac{D_P(z_{max},A,f,h\nu)}{D'_P(A,h\nu)} \tag{6.28}$$

with the geometry shown in Fig. 6.5. Figure 6.5(a) shows measurement of D'_P and Fig. 6.5(b) shows measurement of D_P. The chamber in part (a) is placed at a distance of $f + z_{max}$ from the source.

At low photon energies $z_{max} = 0$, point P is on the surface, and the PSF is referred to as the backscatter factor. The PSF depends on field size A as well as on photon beam energy $h\nu$ and gives the factor by which the radiation dose at

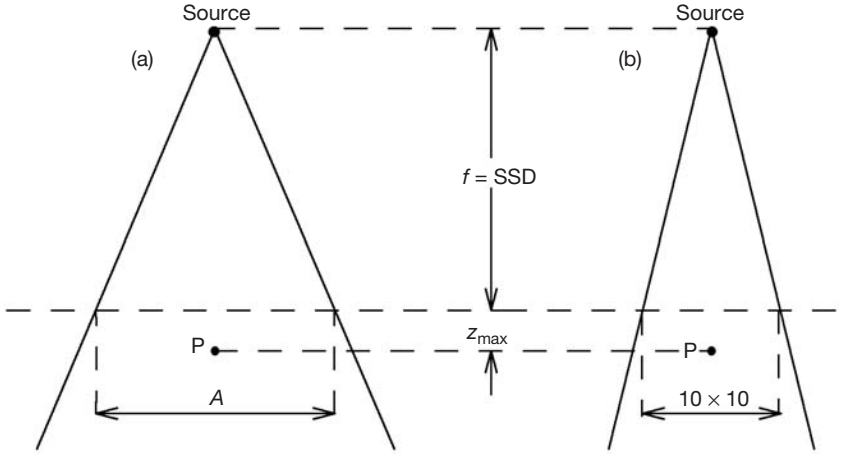

FIG. 6.4. Geometry for measurement of CF(A, hν). The 'dose to small mass of water' is measured at point P in air: in part (a) with field size A, in part (b) with field size 10 × 10 cm². Parameter f stands for the SSD.

point P in air is increased by radiation scattered to point P from the phantom or patient.

Typical values for the PSF range from ~1 for small fields of megavoltage beams, through 1.054 for a 10 × 10 cm^2 field in a cobalt beam to 1.10 for a 50 × 100 cm^2 field in a cobalt beam (used for total body irradiation (TBI)), to 1.50 for a 20 × 20 cm^2 field of orthovoltage X rays (HVL = 1 mm of Cu).

While backscattering is largest at very low photon energies (classical scattering), the energy of backscattered photons is small at low photon energies, causing a rapid absorption of the scattered photons in the medium. At intermediate and high photon energies the backscattering and side scattering decreases with energy; however, the scattered photons have a higher energy and larger penetrating power.

The interrelationship between the amount of backscattering and scattered photon penetration causes the PSF first to increase with beam energy, reaching a peak around HVL ~ 1 mm of Cu, and then to decrease with a further increase in beam energy. The beam quality at which maximum backscatter occurs depends on field size, shifting slightly towards harder radiation with an increase in field size.

For a given beam energy $h\nu$, the PSF increases with field size, as shown in Fig. 6.6 for a ^{60}Co beam.

The scatter factor (SF) (sometimes referred to as relative PSF) for field A is defined as the ratio:

$$\mathrm{SF}(A,h\nu) = \frac{\mathrm{PSF}(A,h\nu)}{\mathrm{PSF}(10,h\nu)} \tag{6.29}$$

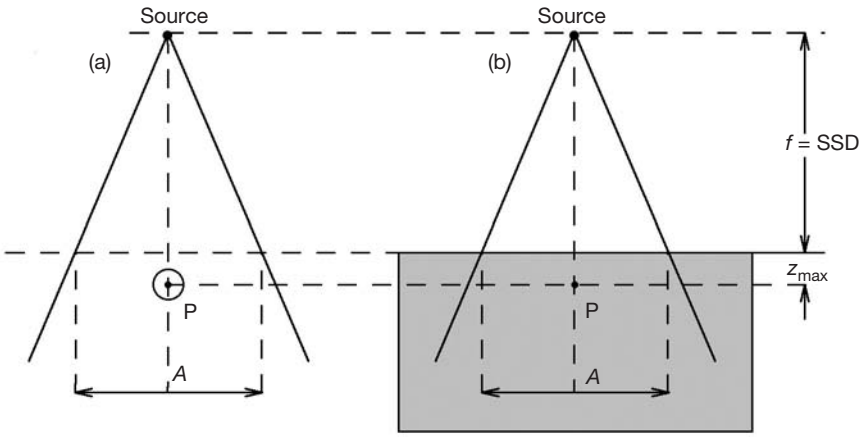

FIG. 6.5. Geometry for measurement of the PSF at point P. (a) The measurement of D'_P; (b) the measurement of D_P. The field size A is the same in (a) and (b).

and thus represents the PSF normalized to 1 for a 10×10 cm^2 field. In Khan's notation the scatter factor is referred to as the phantom scatter factor and is denoted as $S_p(A)$.

6.6.4. Relative dose factor

For a given photon beam at a given SSD, the dose rate at point P (at depth z_{max} in a phantom) depends on the field size A; the larger the field size, the larger the dose. The relative dose factor (RDF) (referred to as the total scatter factor ($S_{c,p}$) in Khan's notation, or sometimes the machine output factor) is defined as the ratio of $D_P(z_{max}, A, f, h\nu)$, the dose at P in a phantom for field A, to $D_P(z_{max}, 10, f, h\nu)$, the dose at P in a phantom for a 10×10 cm^2 field:

$$\mathrm{RDF}(A, h\nu) = S_{c,p}(A, h\nu) = \frac{D_P(z_{max}, A, f, h\nu)}{D_P(z_{max}, 10, f, h\nu)} \tag{6.30}$$

The geometry for measurement of the RDF(A, $h\nu$) is shown in Fig. 6.7(a) for the measurement of $D_P(z_{max}, A, f, h\nu)$ and in Fig. 6.7(b) for the measurement of $D_P(z_{max}, 10, f, h\nu)$.

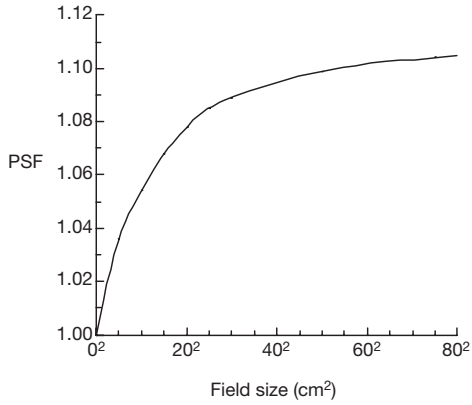

FIG. 6.6. PSF as a function of field size for a ^{60}Co γ ray beam.

From the basic definitions of the CF and the SF we can write RDF as the following product:

$$\mathrm{RDF}(10, h\nu) = \frac{D_{\mathrm{P}}(z_{\max}, A, f, h\nu)}{D_{\mathrm{P}}(z_{\max}, 10, f, h\nu)}$$

$$= \frac{D'_{\mathrm{P}}(A, h\nu)\mathrm{PSF}(A, h\nu)}{D'_{\mathrm{P}}(10, h\nu)\mathrm{PSF}(10, h\nu)} = \mathrm{CF}(A, h\nu)\ \mathrm{SF}(A, h\nu) \qquad (6.31)$$

or in Khan's notation:

$$S_{\mathrm{c,p}}(A, h\nu) = S_{\mathrm{c}}(A, h\nu)S_{\mathrm{p}}(A, h\nu) \qquad (6.32)$$

indicating that the RDF(A) contains two components: scatter from the collimator and scatter from the phantom.

Figure 6.8 shows typical values for the RDF(A, $h\nu$), CF(A, $h\nu$) and SF(A, $h\nu$) against field size A for a ^{60}Co beam. All three functions are normalized to 1 for $A = 10 \times 10$ cm^2; they are larger than 1 for $A > 10 \times 10$ cm^2 and smaller than 1 for $A < 10 \times 10$ cm^2.

When extra shielding is used on an accessories tray or an MLC is used to shape the radiation field on a patient's surface into an irregular field B, then the

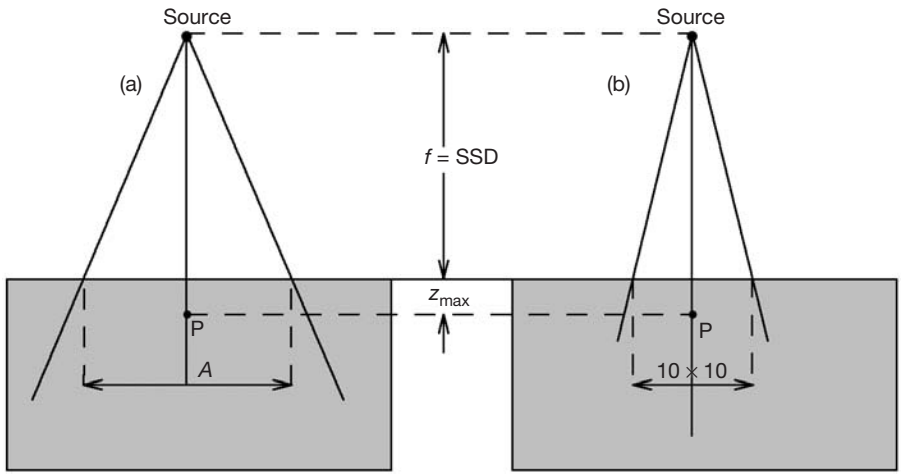

FIG. 6.7. Geometry for the measurement of the RDF(A). The dose at point P at z_{max} in a phantom is measured with field A in part (a) and with field 10 × 10 cm^2 in part (b).

RDF(B, $h\nu$) is in the first approximation given as:

$$\mathrm{RDF}(B, h\nu) = \mathrm{CF}(A, h\nu)\mathrm{SF}(B, h\nu) \tag{6.33}$$

where field A represents the field set by the machine collimator and field B is the actual irregular field on the patient's surface.

We must note that the behaviour of an MLC as a block or a secondary collimator depends on the MLC design and on the manufacturer in the case of linacs, where the MLC replaces the upper or lower collimator jaws. In this case Eq. (6.33) must be used with caution and its validity should be verified before clinical use.

6.7. CENTRAL AXIS DEPTH DOSES IN WATER: SOURCE TO SURFACE DISTANCE SET-UP

6.7.1. Percentage depth dose

Central axis dose distributions inside the patient or phantom are usually normalized to $D_{\max} = 100\%$ at the depth of dose maximum $z_{\max}$ and then

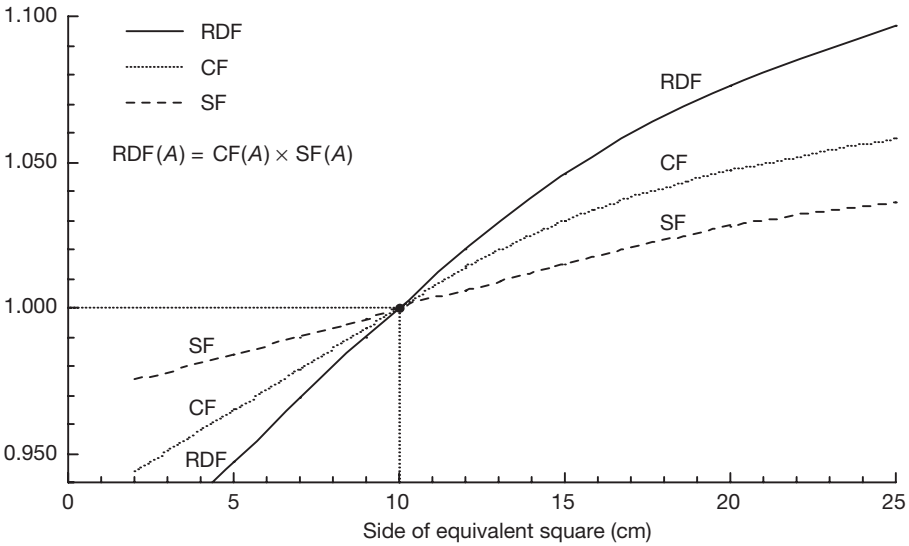

FIG. 6.8. Typical values for the RDF(A), CF(A) and SF(A) for a ^{60}Co γ ray beam as a function of square field size A. All three functions are normalized to 1 for a 10 × 10 cm^2 field.

referred to as the PDD distributions. The PDD is thus defined as follows:

$$\mathrm{PDD}(z, A, f, h\nu) = 100 D_Q / D_P = 100 \dot{D}_Q / \dot{D}_P \tag{6.34}$$

where D_{Q} and $\dot{D}_{\mathrm{Q}}$ are the dose and dose rate, respectively, at point Q at depth z on the central axis of the phantom and D_{P} and $\dot{D}_{\mathrm{P}}$ are the dose and dose rate at point P at $z_{\max}$ on the central axis of the phantom.

The geometry for PDD definition is shown in Fig. 6.9. Point Q is an arbitrary point at depth z on the beam central axis; point P represents the specific dose reference point at $z = z_{\max}$ on the beam central axis. The PDD depends on four parameters: depth in a phantom z, field size A, SSD (often designated with f) and photon beam energy $h\nu$. The PDD ranges in value from 0 at $z \to \infty$ to 100 at $z = z_{\max}$.

The dose at point Q contains two components: primary and scatter.

- The primary component may be expressed as:

$$\mathrm{PDD}^{\mathrm{pri}} = 100 \ \frac{D_{\mathrm{Q}}^{\mathrm{pri}}}{D_{\mathrm{P}}^{\mathrm{pri}}} = 100 \left(\frac{f + z_{\max}}{f + z} \right)^2 e^{-\mu_{\mathrm{eff}}(z - z_{\max})} \tag{6.35}$$

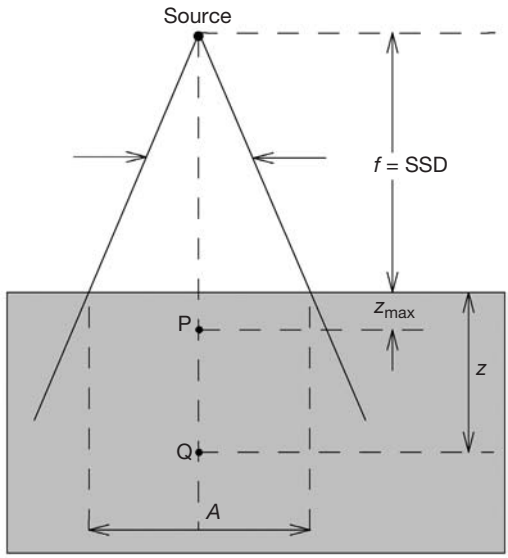

FIG. 6.9. Geometry for PDD measurement and definition. Point Q is an arbitrary point on the beam central axis at depth z, point P is the point at z_{max} on the beam central axis. The field size A is defined on the surface of the phantom.

where μ_{eff} is the effective linear attenuation coefficient for the primary beam in the phantom material (μ_{eff} for a ^{60}Co beam in water is 0.0657 cm^{-1}).

- The scatter component reflects the relative contribution of the scattered radiation to the dose at point Q.

As shown in Fig. 6.3, for constant A, f and $h\nu$ the PDD first increases from the surface to $z = z_{max}$ and then decreases with a further increase in z. The depth of dose maximum and the surface dose depend on the beam energy; the larger the beam energy, the larger the depth of dose maximum and the lower the surface dose.

— For constant z, f and $h\nu$ the PDD increases with increasing A because of increased scatter contribution to points on the central axis. An example for a ^{60}Co beam is given in Table 6.2.
— For constant z, A and $h\nu$ the PDD increases with increasing f because of a decreasing effect of z on the inverse square factor, which governs the primary component of the photon beam. An example for a ^{60}Co beam is given in Table 6.3.
— For constant z, A and f the PDD beyond z_{max} increases with beam energy because of a decrease in beam attenuation (i.e. because of an increase in beam penetrating power).

An example of PDD distributions for 10 × 10 cm^2 fields and various megavoltage photon beams is given in Fig. 6.10 and Table 6.4. The size of the buildup region increases with beam energy and the surface dose decreases with beam energy.

PDDs for radiotherapy beams are usually tabulated for square fields; however, the majority of fields used in radiotherapy are rectangular or irregularly shaped. The concept of equivalent squares is used to determine the square field that will be equivalent to the given rectangular or irregular field.

6.7.2. Scatter function

In radiation dose calculations it is often desirable to separate the scatter component from the total dose at Q:

Scatter component at Q = total dose at Q – primary dose at Q

$$= D'_{P}\text{PSF}(A,h\nu)\text{PDD}(z, A, f, h\nu)/100 - D'_{P}\text{PSF}(0,h\nu)\text{PDD}(z, 0, f, h\nu)/100 \quad (6.36)$$

TABLE 6.2. PERCENTAGE DEPTH DOSES FOR A COBALT-60 BEAM IN WATER FOR VARIOUS FIELD SIZES AND AN SSD OF 100 cm

	A (cm^2)						
	0 × 0	5 × 5	10 × 10	15 × 15	20 × 20	25 × 25	50 × 50
PDD(5, A, 100, Co)	68.2[a]	76.7	80.4	82.0	83.0	83.4	85.2
PDD(10, A, 100, Co)	44.7[a]	53.3	58.7	61.6	63.3	64.4	67.3
PDD(15, A, 100, Co)	29.5[a]	36.5	41.6	44.9	47.1	48.6	49.7

[a] Calculated using Eq. (6.35) with $\mu_{eff} = 0.0657$ cm^{-1}.

TABLE 6.3. PERCENTAGE DEPTH DOSES FOR A COBALT-60 BEAM IN WATER FOR VARIOUS SOURCE TO SURFACE DISTANCES, DEPTH z OF 5 cm IN A PHANTOM AND A FIELD OF A = 10 × 10 cm^2

f = SSD (cm)	60	80	100	120	140
PDD(5, 10, f, Co)	76.2	78.8	80.0	81.3	82.3

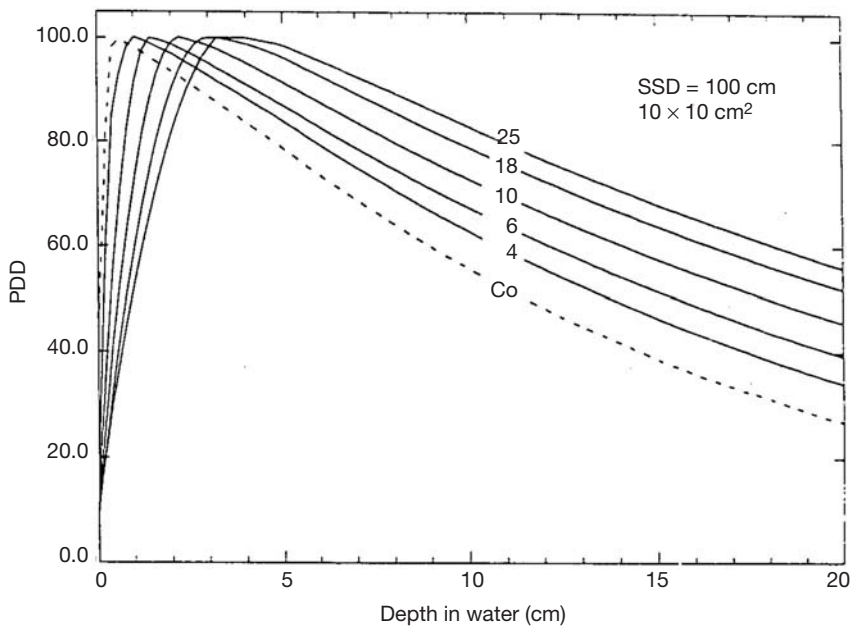

FIG. 6.10. PDD curves in water for a 10 × 10 cm^2 field at an SSD of 100 cm for various megavoltage photon beams ranging from ^{60}Co γ rays to 25 MV X rays.

TABLE 6.4. PERCENTAGE DEPTH DOSES FOR VARIOUS PHOTON BEAMS IN A WATER PHANTOM WITH A FIELD SIZE A OF 10 × 10 cm^2, AN SSD OF 100 cm AND TWO DEPTHS: 5 cm AND 10 cm

	Photon beam $h\nu$					
	Co-60	4 MV	6 MV	10 MV	18 MV	25 MV
Nominal z_{max} (cm)	0.5	1.0	1.5	2.5	3.5	5.0
PDD(5, 10, 100, $h\nu$)	80	84	86	92	97	98
PDD(10, 10, 100, $h\nu$)	59	65	67	74	80	82

The scatter function $S(z, A, f, h\nu)$ is then defined as:

$$S(z, A, f, h\nu) = \text{PSF}(A, h\nu)\text{PDD}(z, A, f, h\nu) - \text{PSF}(0, h\nu)\text{PDD}(z, 0, f, h\nu) \quad (6.37)$$

giving the scatter dose at point Q per 100 cGy of primary dose at point P. Note: PSF(0) = 1 and PDD(z, 0, f, $h\nu$) is the primary PDD calculated with Eq. (6.35).

Similarly to the PDD, the scatter function S also depends on four parameters: depth z, field size A, SSD f and beam energy $h\nu$.

- For constant A, f and $h\nu$ the scatter function S first increases with z, reaches a peak and then slowly decreases, with a further increase in z.
- For constant z, f and $h\nu$, S increases with field size A.
- At $z = z_{max}$ the scatter function S is given by:

$$S(z_{max}, A, f, h\nu) = 100[\text{PSF}(A, h\nu) - 1] \quad (6.38)$$

6.8. CENTRAL AXIS DEPTH DOSES IN WATER: SOURCE TO AXIS DISTANCE SET-UP

When multiple fields are used for the treatment of a particular tumour inside the patient, isocentric (SAD) set-ups are often used because they are more practical in comparison with constant SSD set-ups. Most megavoltage units are mounted isocentrically with an SAD of 80 cm, or more commonly 100 cm, to allow this treatment option. In contrast to SSD set-ups, which rely on PDD distributions, SAD set-ups rely on other functions, such as TARs and tissue–phantom ratios (TPRs), for dosimetric calculations.

6.8.1. Tissue–air ratio

The TAR(z, A_Q, $h\nu$) was originally introduced by Johns to simplify dose calculations in rotational radiotherapy, but its use was subsequently expanded to isocentric irradiations with multiple stationary fields. In rotational radiotherapy the radiation source moves in a circle around the axis of rotation, which is usually inside the tumour. During the rotation around the patient the SSD varies with the patient contour; however, the SAD remains constant.

TAR(z, A_Q, $h\nu$) is defined as the ratio of the dose D_Q or dose rate $\dot{D}_Q$ at point Q on the central axis in the patient or phantom to the dose D'_Q or dose rate $\dot{D}_Q$, the 'dose (rate) to small mass of water in air', at the same point Q on the beam central axis:

$$\mathrm{TAR}(z, A_Q, h\nu) = \frac{D_Q}{D'_Q} = \frac{\dot{D}_Q}{\dot{D}'_Q} \tag{6.39}$$

The geometry for TAR measurement is shown in Fig. 6.11(a) for measurement of D_Q in a phantom and in Fig. 6.11(b) for measurement of D'_Q in air. The field size A_Q is defined at point Q, which is normally placed in the isocentre of the treatment machine.

In contrast to PDD(z, A, f, $h\nu$), which depends on four parameters, TAR(z, A_Q, $h\nu$) depends only on three: depth z, field size A_Q at depth z and

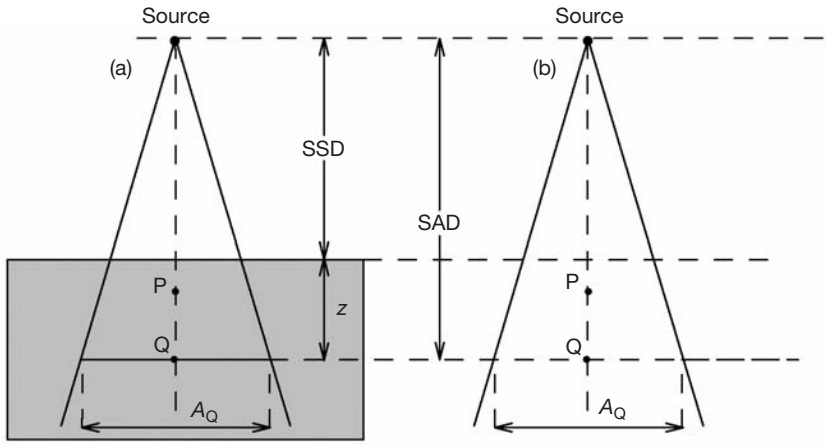

FIG. 6.11. Geometry for measurement and definition of TAR. (a) The dose is determined at point Q in a water phantom; (b) the 'dose to small mass of water' is determined at point Q. Point Q is at the machine isocentre at a distance SAD from the source. The beam field size A_Q is defined at depth z in the phantom.

beam energy $h\nu$; there is essentially no SSD or SAD dependence in the range of SSDs used clinically (50–150 cm). TARs for various ^{60}Co beams at depths of 5 and 10 cm in water are given in Table 6.5.

- For constant A_Q and $h\nu$, the TAR decreases with an increasing z beyond z_{max}.
- For constant z and $h\nu$, the TAR increases with increasing A_Q.
- For constant z and A_Q, the TAR increases with $h\nu$.
- For $z = z_{max}$, the TAR becomes identical to the PSF:

$$\mathrm{TAR}(z = z_{max}, A_Q = A_P, h\nu) = \mathrm{PSF}(A_P, h\nu) \tag{6.40}$$

- The zero area TAR (i.e. TAR(z, 0, $h\nu$) may be calculated from

$$\mathrm{TAR}(z, 0, h\nu) = e^{-\mu_{eff}(z - z_{max})} \tag{6.41}$$

where μ_{eff} is the effective attenuation coefficient for the photon beam $h\nu$. A 0 × 0 field is a hypothetical field in which the dose at depth in a phantom is entirely due to primary photons, since the volume that can scatter radiation is zero.

TARs are most reliably measured with ionization chambers; however, the measurements are much more cumbersome than those of PDDs. In the case of TARs the depth in water must be measured in such a way that the distance between the ionization chamber and the radiation source remains constant, which is difficult to achieve using automatic techniques. Moreover, the measurement of the 'dose to small mass of water' must be carried out with great care in order to ensure full buildup and readings free of radiation scattered into the chamber from the treatment room walls or floor.

Since the concept of 'dose to small mass of medium' is not recommended for use with megavoltage beams above ^{60}Co and 4 MV, the concept of TAR is not used in the dosimetry of medium and high energy photon beams. For these energies functions are used that are similar to the TAR but that do not suffer the limitations imposed on the measurement of the 'dose to small mass of medium'.

6.8.2. Relationship between TAR(d, A_Q, $h\nu$) and PDD(d, A, f, $h\nu$)

As shown in Fig. 6.12, a simple relationship may be derived between TAR(z, A_Q, $h\nu$) and the corresponding PDD(z, A, f, $h\nu$) from the basic

TABLE 6.5. TISSUE–AIR RATIOS FOR A COBALT-60 BEAM IN WATER FOR VARIOUS FIELD SIZES A_Q AND TWO DEPTHS IN A PHANTOM: 5 cm AND 10 cm

	A_Q (cm^2)					
	0 × 0	5 × 5	10 × 10	15 × 15	20 × 20	25 × 25
TAR(5, A_Q, Co)	0.744[a]	0.864	0.921	0.953	0.974	0.986
TAR(10, A_Q, Co)	0.536[a]	0.654	0.731	0.779	0.809	0.831
TAR(20, A_Q, Co)	0.278[a]	0.354	0.418	0.470	0.509	0.536

[a] Calculated using Eq. (6.41) with $\mu_{eff} = 0.0657$ cm^{-1}.

definitions governing the two functions. The basic definitions for the two functions are:

$$\mathrm{TAR}(z, A_Q, h\nu) = \frac{D_Q}{D'_Q} \tag{6.42}$$

$$\mathrm{PDD}(z, A, f, h\nu) = 100\,\frac{D_Q}{D_P} \tag{6.43}$$

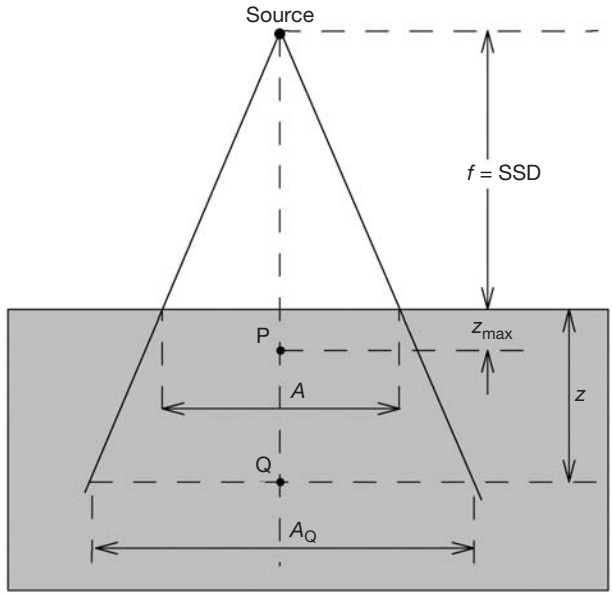

FIG. 6.12. Geometry for the relationship between PDD(z, A, f, hν) and TAR(z, A_Q, hν).

and solving Eqs (6.42) and (6.43) for D_Q we obtain:

$$D_Q = D_P \frac{\text{PDD}(z, A, f, h\nu)}{100} = D'_Q \text{TAR}(z, A_Q, h\nu) \tag{6.44}$$

D_P may now be written as:

$$D_P = D'_P \text{PSF}(A, h\nu) = D'_Q \left(\frac{f + z}{f + z_{max}} \right)^2 \text{PSF}(A, h\nu) \tag{6.45}$$

and inserted into Eq. (6.44) to yield:

$$\text{TAR}(z, A_Q, h\nu) = \text{PSF}(A, h\nu) \frac{\text{PDD}(z, A, f, h\nu)}{100} \left(\frac{f + z}{f + z_{max}} \right)^2 \tag{6.46}$$

For the special case of $z = z_{max}$, where PDD(z_{max}, A, f, $h\nu$) = 100, Eq. (6.46) shows that the PSF(A, $h\nu$) is a special TAR(z_{max}, A, $h\nu$). The range of TARs is therefore from 0 at $z \to \infty$ to PSF(A, $h\nu$) at $z = z_{max}$.

Since the TAR does not depend on the SSD, a single TAR table for a given photon beam energy may be used to cover all possible SSDs used clinically.

Alternatively, PDDs for any arbitrary combination of z, A and f = SSD may be calculated from a single TAR table.

Based on Eq. (6.46) we derive the following two relationships for PDDs at two different SSDs (f_1 and f_2).

- The first relationship assumes an identical field size A at the two SSDs, as shown in Fig. 6.13:

$$\frac{\text{PDD}(z, A, f_1, h\nu)}{\text{PDD}(z, A, f_2, h\nu)} = \left(\frac{\text{TAR}(z, A_{Q1}, h\nu)}{\text{TAR}(z, A_{Q2}, h\nu)} \right) \left(\frac{\frac{f_1 + z_{max}}{f_1 + z}}{\frac{f_2 + z_{max}}{f_2 + z}} \right)^2 \tag{6.47}$$

- The second relationship assumes the same field size A_Q at depth z at the two SSDs, as shown in Fig. 6.14:

$$\frac{\mathrm{PDD}(z, A_1, f_1, h\nu)}{\mathrm{PDD}(z, A_2, f_2, h\nu)} = \left(\frac{\mathrm{PSF}(A_2, h\nu)}{\mathrm{PSF}(A_1, h\nu)}\right)\left(\frac{\dfrac{f_1 + z_{\max}}{f_1 + z}}{\dfrac{f_2 + z_{\max}}{f_2 + z}}\right)^2 \tag{6.48}$$

The relationships in Eqs (6.47) and (6.48) consist of two components each; the inverse square law correction component is the main component of the correction, and is referred to as the Mayneord factor. The second factor, represented by the ratio of TARs or PSFs, is often ignored, because its effect is much smaller than that produced by the Mayneord factor, and the Mayneord factor alone is used for correction of PDDs from one SSD to another.

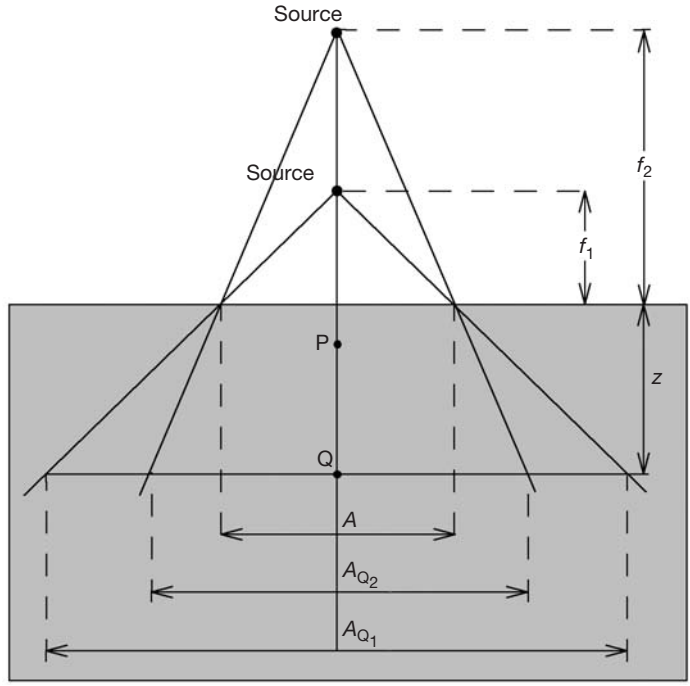

FIG. 6.13. Derivation of the PDD relationship for two SSDs, with field size A identical for both. Note that the field A on the phantom surface is the same for both SSDs; therefore the fields at depth z differ for the two SSDs but are related through simple geometrical relationships.

6.8.3. Scatter–air ratio

Just as it was convenient in dealing with PDDs to separate the scattered component from the primary component to obtain the scatter function, it is sometimes useful to separate the primary component of the TAR from the total TAR to obtain the scatter contribution, which, in this case, is referred to as the scatter–air ratio (SAR), defined as:

$$\mathrm{SAR}(z, A_Q, h\nu) = \mathrm{TAR}(z, A_Q, h\nu) - \mathrm{TAR}(z, 0, h\nu) \tag{6.49}$$

The SAR depends on the same three parameters as the TAR and gives the scatter contribution to the dose at point Q in a phantom per 1 cGy of dose to a small mass of water at point Q in air.

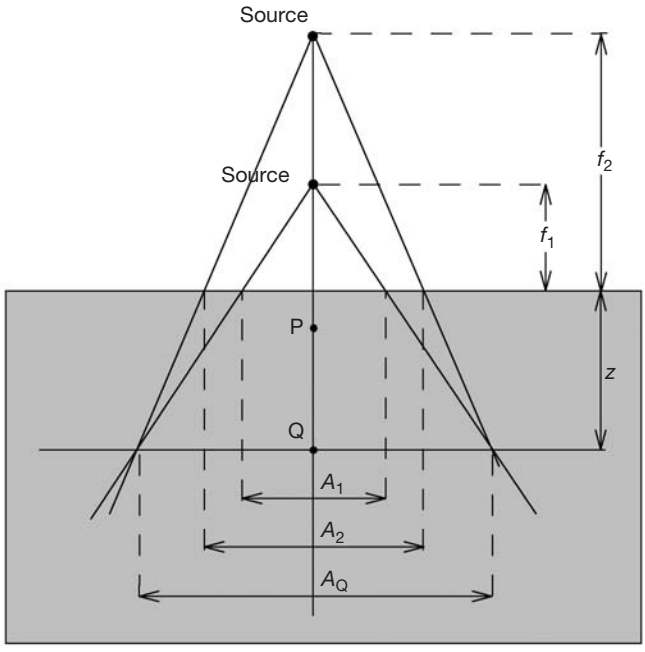

FIG. 6.14. Derivation of the PDD relationship for two SSDs with field size A_Q identical for both. Here the fields A_1 and A_2 on the phantom surface are related through simple geometrical relationships.

6.8.4. Relationship between SAR (d, A_Q, $h\nu$) and $S(z, A, f, h\nu)$

Similarly to the relationship between TAR(z, A_Q, $h\nu$) and PDD(z, A, f, $h\nu$), we can derive the relationship between SAR(z, A_Q, $h\nu$) and $S(z, A, f, h\nu)$ to obtain:

$$\mathrm{SAR}(z, A_Q, h\nu) = \frac{S(z, A, f, h\nu)}{100} \left(\frac{f + z}{f + z_{max}} \right)^2 \tag{6.50}$$

It is easy to see that:

$$S(z, A, f, h\nu) = 100\mathrm{SAR}(z, A_Q, h\nu) \tag{6.51}$$

for any z when $f \to \infty$ and for any f when $z \to z_{max}$.

6.8.5. Tissue–phantom ratio and tissue–maximum ratio

The TAR concept works well in isocentric set-ups for photon energies of ^{60}Co and below. For megavoltage X rays produced by high energy linacs, however, the concept breaks down because of difficulties in measuring the 'dose to small mass of water in air' at those energies (the required size of the buildup cap for the ionization chamber becomes excessively large). To bypass this problem, the concept of tissue–phantom ratio (TPR) was introduced for use in megavoltage isocentric set-ups.

The TPR is defined as follows:

$$\mathrm{TPR}(z, A_Q, h\nu) = \frac{D_Q}{D_{Qref}} = \frac{\dot{D}_Q}{\dot{D}_{Qref}} \tag{6.52}$$

where D_Q and $\dot{D}_Q$ are the dose and dose rate, respectively, in a phantom at arbitrary point Q on the beam central axis and D_{Qref} and $\dot{D}_{Qref}$ are the dose and dose rate, respectively, in a phantom at a reference depth z_{ref} (typically 5 or 10 cm) on the beam central axis.

The geometry for the measurement of doses D_Q and D_{Qref} is shown in Fig. 6.15.

A special TPR was defined for the reference depth z_{ref} equal to the depth of dose maximum z_{max}, which is referred to as the tissue–maximum ratio (TMR), defined as follows:

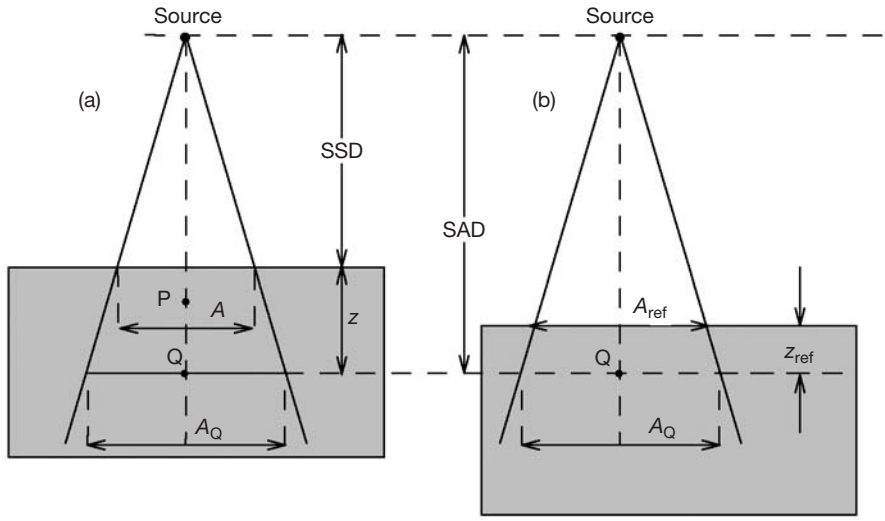

FIG. 6.15. Geometry for measurement of TPR(d, A_Q, hν). (a) The geometry for the measurement of D_Q at depth z in a phantom; (b) the geometry for the measurement of D_{Qref} at depth z_{ref} in a phantom. The distance between the source and the point of measurement, as well as the field size at the point of measurement, is the same for (a) and (b).

$$\mathrm{TMR}(z, A_\mathrm{Q}, h\nu) = \frac{D_\mathrm{Q}}{D_\mathrm{Qmax}} = \frac{\dot{D}_\mathrm{Q}}{\dot{D}_\mathrm{Qmax}} \tag{6.53}$$

where D_Q and $\dot{D}_\mathrm{Q}$ are the dose and dose rate, respectively, at point Q at a depth z in a phantom and D_Qmax and $\dot{D}_\mathrm{Qmax}$ are the dose and dose rate, respectively, at point Q at z_max.

The geometry for the definition of TMR is the same as in Fig. 6.15, except that z_ref is now z_max.

- Just like the TAR, the TPR and TMR depend on the three parameters z, A_Q, $h\nu$, but do not depend on the SAD or SSD.
- The range of TMR is from 0 for $z \to \infty$ to 1 for $z = z_\mathrm{max}$ (i.e. $0 \leq \mathrm{TMR}(z, A_\mathrm{Q}, h\nu) \leq 1$.
- For constant A_Q and $h\nu$ the TMR decreases with increasing z.
- For constant z and $h\nu$ the TMR increases with increasing A_Q.
- For constant z and A_Q the TMR increases with increasing $h\nu$.

6.8.6. Relationship between TMR(z, A_Q, $h\nu$) and PDD(z, A, f, $h\nu$)

As shown in Fig. 6.16, a simple relationship may be derived between TMR(z, A_Q, $h\nu$) and the corresponding PDD(z, A, f, $h\nu$) from the basic definitions governing the two functions.

The basic definitions for the two functions are:

$$\mathrm{TMR}(z, A_Q, h\nu) = \frac{D_Q}{D_{Q\max}} \tag{6.54}$$

$$\mathrm{PDD}(z, A, f, h\nu) = 100\frac{D_Q}{D_P} \tag{6.55}$$

Solving Eqs (6.54) and (6.55) for D_Q we obtain:

$$D_Q = D_P \frac{\mathrm{PDD}(z, A, f, h\nu)}{100} = D_{Q\max}\mathrm{TMR}(z, A_Q, h\nu) \tag{6.56}$$

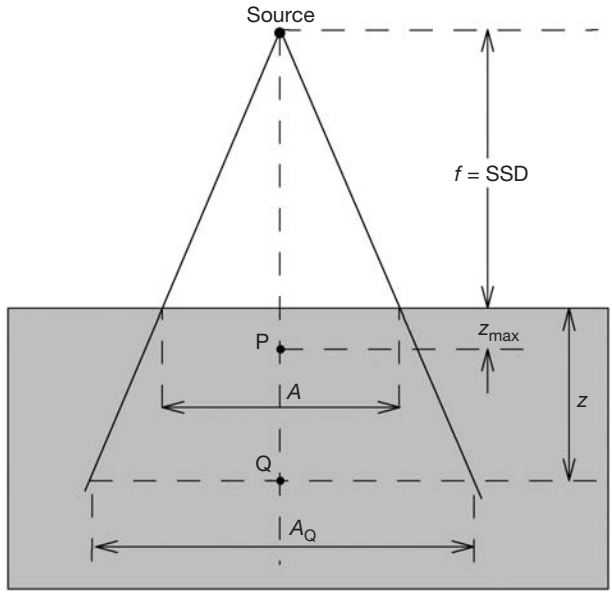

FIG. 6.16. Geometry for derivation of the relationship between PDD(z, A, f, hν) and TMR(z, A_Q, hν).

and expanding D_P and D_{Qmax} as follows:

$$D_P = D'_P \text{PSF}(A, h\nu) = D'_Q \left(\frac{f+z}{f+z_{max}} \right)^2 \text{PSF}(A, h\nu) \tag{6.57}$$

$$D_{Qmax} = D'_Q \ \text{PSF}(A_Q, h\nu) \tag{6.58}$$

we obtain:

$$\text{TMR}(z, A_Q, h\nu) = \frac{\text{PDD}(z, A, f, h\nu)}{100} \ \frac{\text{PSF}(A, h\nu)}{\text{PSF}(A_Q, h\nu)} \left(\frac{f+z}{f+z_{max}} \right)^2 \tag{6.59}$$

In the first approximation, ignoring the PSF ratio in Eq. (6.59), we have a very simple approximate relationship between TMR(z, A_Q, $h\nu$) and PDD(z, A, f, $h\nu$) as:

$$\text{TMR}(z, A_Q, h\nu) \approx \frac{\text{PDD}(z, A, f, h\nu)}{100} \left(\frac{f+z}{f+z_{max}} \right)^2 \tag{6.60}$$

The error in ignoring the ratio PSF(A, $h\nu$)/PSF(A_Q, $h\nu$) is very small and can be estimated easily for a cobalt beam. For an extreme example, take the case with depth in a phantom d = 20 cm, field size A = 20 × 20 cm^2 and SSD f = 100 cm to obtain A_Q = 24 × 24 cm^2 and PSF(20, Co)/PSF(24, Co) = 1.078/1.083 = 0.995, or a 0.5% error. Errors for smaller fields and shorter SSDs are obviously smaller, making Eq. (6.60) a reasonable and very practical approximation for relating the TMR with the PDD.

6.8.7. Scatter–maximum ratio

Similarly to separating TAR(z, A_Q, $h\nu$) into the primary component TAR(z, 0, $h\nu$) and the scatter component SAR(z, A_Q, $h\nu$), the TMR(z, A_Q, $h\nu$) can be separated into the primary component TMR(z, 0, $h\nu$) and the scatter component, referred to as the scatter–maximum ratio (SMR), defined as follows:

$$\text{SMR}(z, A_Q, h\nu) = \text{TMR}(z, A_Q, h\nu) \frac{\text{SF}(A_Q, h\nu)}{\text{SF}(0, h\nu)} - \text{TMR}(z, 0, h\nu) \tag{6.61}$$

where SF(A_Q, $h\nu$) and SF(0, $h\nu$) are the scatter factors for fields A_Q and 0, respectively, and photon energy $h\nu$, as defined in Eq. (6.29).

The ratio SF(A_Q, $h\nu$)/SF(0, $h\nu$) is therefore:

$$\frac{\mathrm{SF}(A_Q, h\nu)}{\mathrm{SF}(0, h\nu)} = \frac{\mathrm{PSF}(A_Q, h\nu)/\mathrm{PSF}(10, h\nu)}{\mathrm{PSF}(0, h\nu)/\mathrm{PSF}(10, h\nu)} = \mathrm{PSF}(A_Q, h\nu) \tag{6.62}$$

since PSF(0, $h\nu$) = 1.

For ^{60}Co γ rays, SMRs are approximately the same as SARs. However, for megavoltage photon energies above ^{60}Co the SMRs should be calculated from the TMRs using Eq. (6.61) and:

$$\mathrm{TMR}(z, 0, h\nu) = e^{-\mu_{\mathrm{eff}}(z - z_{\max})} \tag{6.63}$$

where μ_{eff} is the effective attenuation coefficient for the photon beam $h\nu$.

6.9. OFF-AXIS RATIOS AND BEAM PROFILES

Dose distributions along the beam central axis give only part of the information required for an accurate dose description inside the patient. Dose distributions in 2-D and 3-D are determined with central axis data in conjunction with off-axis dose profiles.

In the simplest form, the off-axis data are given with beam profiles measured perpendicularly to the beam central axis at a given depth in a phantom. The depths of measurement are typically at $z_{\max}$ and 10 cm for verification of compliance with machine specifications, in addition to other depths required by the particular treatment planning system (TPS) used in the department. An example of typical dose profiles measured at various depths in water for two field sizes (10 × 10 and 30 × 30 cm^2) and a 10 MV X ray beam is shown in Fig. 6.17.

Combining a central axis dose distribution with off-axis data results in a volume dose matrix that provides 2-D and 3-D information on the dose distribution. The off-axis ratio (OAR) is usually defined as the ratio of dose at an off-axis point to the dose on the central beam axis at the same depth in a phantom.

Megavoltage X ray beam profiles consist of three distinct regions: central, penumbra and umbra.

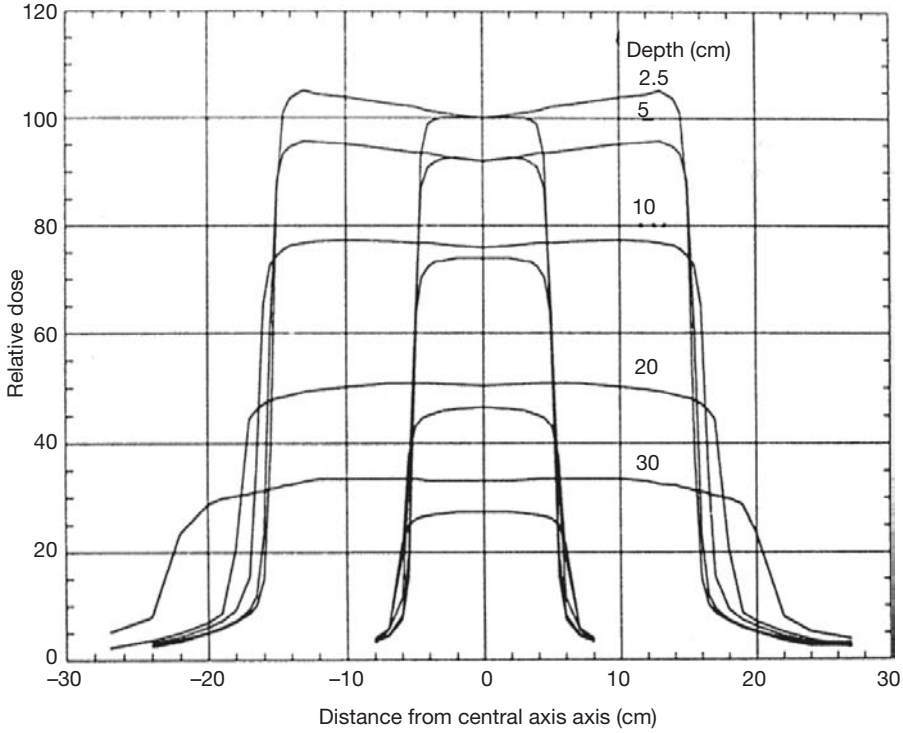

FIG. 6.17. An example of beam profiles for two field sizes (10 × 10 cm^2 and 30 × 30 cm^2) and a 10 MV X ray beam at various depths in water. The central axis dose values are scaled by the appropriate PDD value for the two fields.

- The central region represents the central portion of the profile extending from the beam central axis to within 1–1.5 cm from the geometric field edges of the beam. The geometric field size, indicated by the optical light field, is usually defined as the separation between the 50% dose level points on the beam profile. In the central region, the beam profile for ^{60}Co beams is affected by the inverse square dose fall-off as well as by increased phantom thickness for off-axis points. For linacs, on the other hand, the central region of the beam profile is affected by the energy of electrons striking the thick target, by the target atomic number and by the flattening filter atomic number and geometric shape.
- In the penumbral region of the dose profile the dose changes rapidly and depends also on the field defining collimators, the finite size of the focal spot (source size) and the lateral electronic disequilibrium. The dose fall-off around the geometric beam edge is sigmoid in shape and extends

under the collimator jaws into the penumbral tail region, where there is a small component of dose due to the transmission through the collimator jaws (transmission penumbra), a component attributed to finite source size (geometric penumbra) and a significant component due to in-patient X ray scatter (scatter penumbra). The total penumbra is referred to as the physical penumbra and is the sum of the three individual penumbras: transmission, geometric and scatter. The physical penumbra depends on beam energy, source size, SSD, source to collimator distance and depth in a phantom.

- Umbra is the region outside the radiation field, far removed from the field edges. The dose in this region is generally low and results from radiation transmitted through the collimator and head shielding.

Dose profile uniformity is usually measured by a scan along the centre of both major beam axes for various depths in a water phantom. Two parameters that quantify field uniformity are then determined: field (beam) flatness and field (beam) symmetry.

6.9.1. Beam flatness

The beam flatness F is assessed by finding the maximum D_{max} and minimum D_{min} dose point values on the beam profile within the central 80% of the beam width and then using the relationship:

$$F = 100 \times \frac{D_{max} - D_{min}}{D_{max} + D_{min}} \tag{6.64}$$

Standard linac specifications generally require that F be less than 3% when measured in a water phantom at a depth of 10 cm and an SSD of 100 cm for the largest field size available (usually 40×40 cm^2).

Compliance with the flatness specifications at a depth of 10 cm in water results in 'over-flattening' at z_{max}, which manifests itself in the form of 'horns' in the profile, and in 'under-flattening', which progressively worsens as the depth z increases from 10 cm to larger depths beyond 10 cm, as evident from the profiles for the 30×30 cm^2 field in Fig. 6.17. The typical limitation on beam horns in the z_{max} profile is 5% for a 40×40 cm^2 field at SSD = 100 cm. The over-flattening and under-flattening of the beam profiles is caused by the lower beam effective energies in off-axis directions compared with those in the central axis direction.

6.9.2. Beam symmetry

The beam symmetry S is usually determined at z_{max}, which represents the most sensitive depth for assessment of this beam uniformity parameter. A typical symmetry specification is that any two dose points on a beam profile, equidistant from the central axis point, are within 2% of each other. Alternately, areas under the z_{max} beam profile on each side (left and right) of the central axis extending to the 50% dose level (normalized to 100% at the central axis point) are determined and S is then calculated from:

$$S = 100 \times \frac{\text{area}_{\text{left}} - \text{area}_{\text{right}}}{\text{area}_{\text{left}} + \text{area}_{\text{right}}} \tag{6.65}$$

The areas under the z_{max} profiles can often be determined using an automatic option on the water tank scanning device (3-D isodose plotter). Alternatively, using a planimeter or even counting squares on graph paper with a hard copy of the profile are practical options.

6.10. ISODOSE DISTRIBUTIONS IN WATER PHANTOMS

The physical characteristics of radiation beams are usually measured in phantoms under standard conditions that are as follows:

- A homogeneous, unit density phantom;
- A flat phantom surface;
- A perpendicular beam incidence on the phantom.

The central axis depth dose data in conjunction with dose profiles contain complete 2-D and 3-D information about a radiation beam. However, this information is difficult to visualize even for a single beam, let alone for a combination of several beams.

Planar and volumetric variations in depth doses are usually displayed by means of isodose curves or isodose surfaces, which connect points of equal dose in a volume of interest. The isodose curves and surfaces are usually drawn at regular intervals of absorbed dose and are expressed as a percentage of the dose at a specific reference point.

An isodose chart for a given single beam consists of a family of isodose curves usually drawn at regular increments of PDD. Two normalization conventions are in use:

— For SSD set-ups, all isodose values are normalized to 100 at point P on the central beam axis.
— For SAD set-ups, the isodose values are normalized to 100 at the isocentre.

The isodose charts for an SSD set-up are thus plots of PDD values, while isodose charts for an SAD set-up are plots of either TAR or TMR values.

For a ^{60}Co beam the dose at any depth is largest on the central beam axis and then decreases towards the beam edges. For megavoltage photon beams the off-axis dose at shallow depths is usually larger than the central axis dose at the same depth, as a consequence of flattening filter design. These filters provide flat beams at a depth of 10 cm in water, and to achieve this they must overcompensate at shallow depths. (Note that the effective beam energy in extreme off-axis directions is lower than the effective beam energy in the direction of the central beam axis.)

Figure 6.18 shows an example of isodose charts for a ^{60}Co beam in water: Fig. 6.18(a) shows an SSD set-up (A = 10 × 10 cm^2; SSD = 80 cm); Fig. 6.18(b) shows an SAD set-up (A_Q = 10 × 10 cm^2; SAD = 100 cm; depth of isocentre = 10 cm).

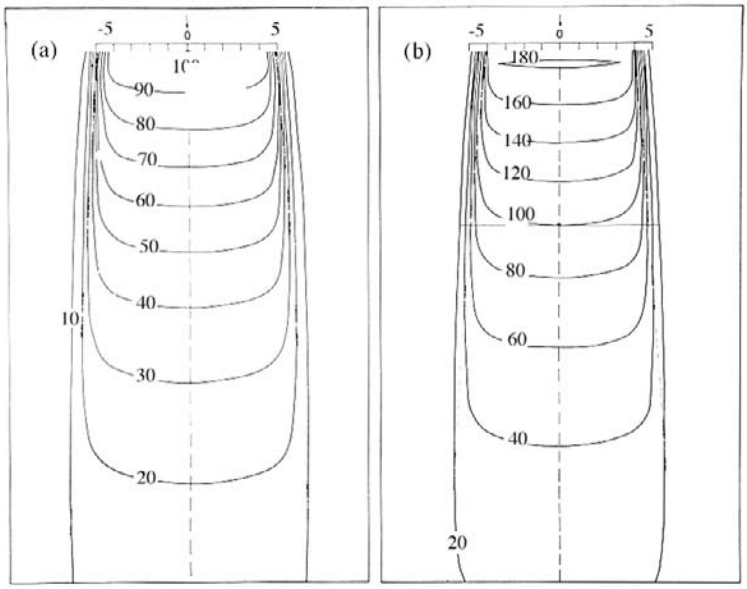

FIG. 6.18. Isodose curves for a ^{60}Co γ ray beam: (a) for an SSD set-up (A = 10 × 10 cm^2; SSD = 80 cm) and (b) for an SAD set-up (A_Q=10 × 10 cm^2, SAD = 100 cm; depth of isocentre = 10 cm).

Near the beam edges in the penumbra region the dose decreases rapidly with lateral distance from the beam central axis. This dose fall-off is caused not only by the geometric penumbra but also by the reduced side scatter.

Outside the geometric limits of the beam and the penumbra, the dose variation is the result of three components:

(i) Scatter from the radiation field;
(ii) Leakage through the collimator jaws and machine head housing;
(iii) Scatter from the collimation system.

Parameters that affect the single beam isodose distribution are beam quality, source size, beam collimation, field size, SSD and source to collimator distance.

Isodose charts are measured with ionization chambers, solid state detectors, standard radiographic film and radiochromic film.

In addition to direct measurements, isodose charts may also be generated by calculations using various algorithms for treatment planning, most commonly with commercially available TPSs.

Treatment by a single photon beam is seldom used except for superficial tumours. Deep seated tumours are usually treated with a combination of two or more beams so as to achieve an acceptable dose distribution within the tumour and the surrounding normal tissues (see Chapter 7). As a rule, the tumour dose is higher than the dose to the surrounding normal tissues, and the dose distribution within the tumour should be homogeneous to within +7% and –5% of the prescribed dose, if at all possible.

6.11. SINGLE FIELD ISODOSE DISTRIBUTIONS IN PATIENTS

In clinical situations the beam may be obliquely incident on the patient and the patient's surface may be curved or of irregular shape, requiring corrections for contour irregularities. In addition, some irradiated tissues, such as lung and bone, have densities that differ considerably from that of water, requiring corrections for tissue heterogeneities.

Isodose distributions in patients are determined by one of two radically different approaches:

- Correction based algorithms;
- Model based algorithms.

Correction based algorithms use depth dose data measured in water phantoms with a flat surface and normal incidence in conjunction with various methods to correct for irregular patient contours and oblique beam incidence, in contrast to the flat surface of a water phantom. They also correct for organ inhomogeneities to account for varying electron densities of organs, in contrast to the uniform electron density of a water phantom.

Model based algorithms obviate the correction problem by modelling the dose distributions from first principles and accounting for all geometrical and physical characteristics of the particular patient treatment.

Before clinical use both correction algorithms and model based algorithms must be verified experimentally, which often is a difficult task. The relative importance of individual corrections varies with the particular treatment geometry and the position of the target volume inside the patient. For conventional treatment techniques the correction based algorithms work reasonably well and produce reliable dose distributions; however, for the new sophisticated treatments such as 3-D conformal radiotherapy and intensity modulated radiotherapy (IMRT), they become problematic, because of the radical corrections that are required for these techniques. Model based algorithms hold great promise for the future; however, they are currently still under development.

6.11.1. Corrections for irregular contours and oblique beam incidence

A radiation beam striking an irregular or sloping patient surface produces an isodose distribution that differs from the standard distributions obtained on flat surfaces with a normal beam incidence. Two approaches are used to address this problem:

- The effect can be corrected through various calculation methods;
- The effect may be compensated for through the use of wedges, bolus materials or compensators.

Several methods have been developed to correct standard flat surface/normal incidence isodose distributions for contour irregularities and oblique angles of beam incidence. The three most commonly used methods, applicable for angles of incidence up to 45º for megavoltage X ray beams and up to 30º for orthovoltage X ray beams, are:

— The effective SSD method;
— The TAR or TMR method;
— The isodose shift method.

The correction factors for these three methods can be understood with reference to Fig. 6.19, in which an irregular patient contour CC is treated with a beam with an SSD = *f*. The PDD at point S normalized to dose at point P on the beam central axis is referred to as PDD_{corr} and is calculated with one of the three methods listed above.

6.11.1.1. Effective source to surface distance method

In the effective SSD method, PDD_{corr} is determined from:

$$PDD_{corr} = PDD'(z, A, f, h\nu)\left(\frac{f + z_{max}}{f + h + z_{max}}\right)^2 \quad (6.66)$$

where $PDD'(z, A, f, h\nu)$ is the PDD under standard conditions with the flat surface C′C′ and the second term represents an inverse square correction factor. The parameter *h* is the thickness of missing tissue, while the parameter – *h* represents the thickness of excess tissue. An assumption is made that the PDD does not depend on the SSD for deviations from the nominal SSD of the

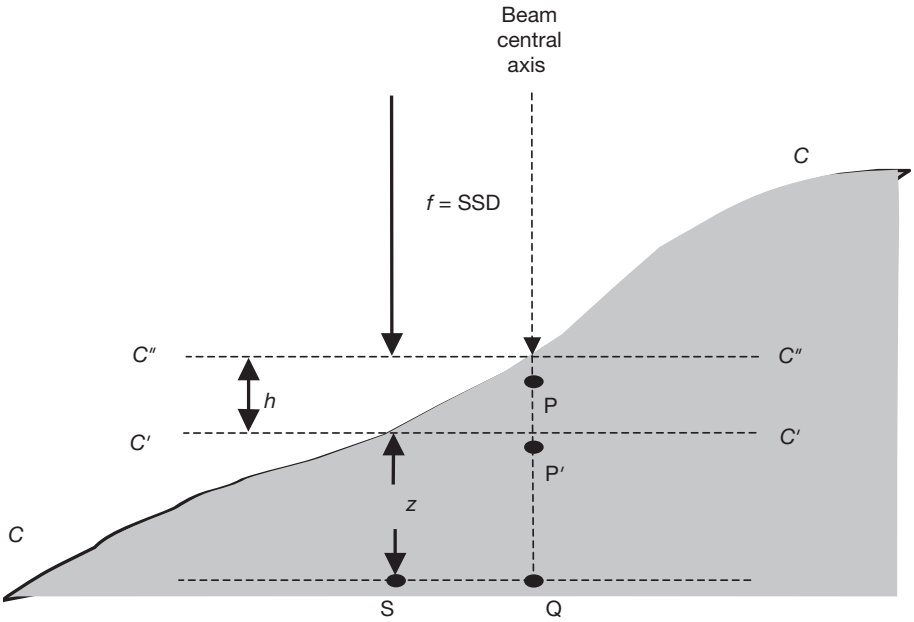

FIG. 6.19. Geometry used for dose determination at point S in a patient. CC represents the actual patient contour; C′C′ and C″C″ are flat phantom contours: C″C″ at the nominal SSD and C′C′ at SSD + h, where h represents the thickness of missing tissue directly above point S. Point P is the point of dose normalization at z_{max} on the central beam axis.

order of h (i.e. $h << f$). The resulting PDD is normalized to 100 at point P on the central beam axis.

Thus in the effective SSD method (see Fig. 6.19): (a) the isodose chart is shifted to the flat surface level at the C′C′ contour; (b) the PDD value for point S is read; and (c) the reading is corrected by an inverse square law factor.

6.11.1.2. Tissue–air ratio or tissue–maximum ratio method

In the TAR or TMR method, PDD_{corr} is given as:

$$PDD_{corr} = PDD''(z+h, A, f, h\nu)\ \frac{T(z, A_Q, h\nu)}{T(z+h, A_Q, h\nu)} \tag{6.67}$$

where

A_Q is the field size at point S at a distance $(f + h + z)$ from the source.
T stands for either the TAR or the TMR, and an assumption is made that TARs and TMRs do not depend on the SSD.
PDD″ represents the PDD value at depth $(h + z)$ for a standard flat phantom with the surface at C″C″.
h is missing or excessive tissue. For missing tissue h is positive, for excess tissue h is negative.

6.11.1.3. Isodose shift method

In the isodose shift method, the value of the dose at S is shifted on a vertical ray line by $(h \times k)$, where h is the thickness of the missing or excess tissue and k is a factor depending on beam energy. The factor k is smaller than 1 and has a value of 0.7 for ^{60}Co beams to 5 MV beams, 0.6 for 5–15 MV beams and 0.5 for 15–30 MV beams. For missing tissue h is positive and the isodose is shifted away from the source, while for excess tissue h is negative and the isodose is shifted towards the source.

6.11.2. Missing tissue compensation

In addition to techniques to correct for contour irregularities and oblique beam incidence, as discussed in Section 6.11.1, many relatively simple techniques have been devised to compensate for missing tissue, most notably the use of wedges, bolus materials and compensators.

6.11.2.1. Wedge filters

Wedge filters may be used to even out the isodose surfaces for photon beams striking relatively flat patient surfaces under an oblique beam incidence.

Two types of wedge filter are in use: physical wedge filters and dynamic wedge filters.

- Physical wedges are made of lead, brass or steel. When placed in a radiation beam, they cause a progressive decrease in the intensity across the beam and a tilt of isodose curves under normal beam incidence.
- Dynamic wedges provide the wedge effect on isodose curves through a closing motion of a collimator block during irradiation.

The wedge angle is defined as the angle through which an isodose curve at a given depth in water (usually 10 cm) is tilted at the central beam axis under the condition of normal beam incidence.

Physical wedges are usually available with wedge angles of 15º, 30º, 45º and 60º; dynamic wedges are available with any arbitrary wedge angle in the range 0–60º.

The wedge (transmission) factor (WF) is defined as the ratio of doses at z_{max} in a water phantom on the beam central axis with and without the wedge.

Physical wedge filters may alter the X ray beam quality, causing beam hardening at energies of 6–10 MV and beam softening at energies above 15 MV. These effects will affect the central axis PDDs and should be accounted for in treatment planning isodose distribution calculations.

6.11.2.2. Bolus

Bolus is a tissue equivalent material placed directly on the skin surface to even out the irregular patient contour and thereby provide a flat surface for normal beam incidence. In principle, the use of bolus is straightforward and practical; however, it suffers a serious drawback: for megavoltage photon beams it results in the loss of the skin sparing effect in the skin under the bolus layer (i.e. skin sparing occurs in the bolus).

6.11.2.3. Compensators

Compensators are used to produce the same effect as the bolus yet preserve the skin sparing effect of megavoltage photon beams. They are custom-made devices that mimic the shape of the bolus but are placed in the radiation beam at some 15–20 cm from the skin surface so as not to disrupt the

skin sparing properties of the beam. Although compensators may be made of water equivalent materials, they are usually fabricated from lead or special low melting point alloys, such as Cerrobend (Lipowitz's metal).

Since compensators are placed at some distance from the skin surface so as not to affect the skin dose sparing, their shape must be adjusted for:

— Beam divergence;
— Linear attenuation coefficients of the compensator material relative to that of water;
— Reduction in scatter at various depths when the compensator is placed in the radiation beam away from the skin surface rather than in contact with the skin.

6.11.3. Corrections for tissue inhomogeneities

Standard isodose charts and depth dose tables are given for uniform density water phantoms. Radiation beams used in patient treatment, however, traverse various tissues that may differ from water in density and atomic number. These tissue inhomogeneities (also referred to as heterogeneities) affect the dose deposition in the patient and may result in isodose distributions that differ considerably from those obtained in water phantoms. The effects of inhomogeneities on radiation dose distributions depend on the amount, density and atomic number of the inhomogeneity, as well as on the quality of the photon beam, and may be separated into two distinct categories:

- Increase or decrease in the attenuation of the primary beam, which affects the distribution of the scattered radiation;
- Increase or decrease of the secondary electron fluence.

Three separate regions, in addition to inhomogeneity boundaries, are considered with regard to inhomogeneities: (1) the point of interest P located in front of the inhomogeneity; (2) P inside the inhomogeneity; and (3) P beyond the inhomogeneity.

In region (1), in front of the inhomogeneity, especially for megavoltage photon beams, the dose is not affected by the inhomogeneity, since the primary beam in this region is not affected and neither is the scatter component, except close to the boundary.

In region (2) the dose is mainly affected by changes in the secondary electron fluence and to a lesser extent by changes in the primary beam attenuation in the inhomogeneity. Under the conditions of electronic equilibrium and for a given photon energy fluence, the ratio of absorbed doses

in two different media is equal to the ratio of mass–energy absorption coefficients for the two media. Close to the soft tissue–lung interfaces there may be a partial loss of electronic equilibrium and an associated decrease in dose.

In region (3), beyond the inhomogeneity, the dose is mainly affected by changes in the primary beam attenuation and to a lesser extent by changes in scatter. Four empirical methods (see Section 7.5.6) are available for correcting the water phantom dose to estimate the dose at points in region (3):

— The TAR method;
— The power law TAR method;
— The equivalent TAR method;
— The isodose shift method.

Beyond healthy lung (density ~0.3 g/cm^3) the dose in soft tissues will increase, while beyond bone (density ~1.6 g/cm^3) it will decrease in comparison with dose measured in a uniform phantom.

Typical corrections for dose beyond healthy lung are: 4%, 3%, 2% and 1% per centimetre of lung for ^{60}Co γ beams and 4, 10 and 20 MV X rays, respectively.

The shielding effect of bone depends strongly on the beam energy; it is appreciable at low X ray energies because of a strong photoelectric effect presence and essentially negligible in the low megavoltage energy range (mainly Compton effect). At energies above 10 MeV the shielding effect of bone begins to increase with increasing energy because of the increase in the pair production cross-section.

6.11.4. Model based algorithms

Model based algorithms for computation of dose distributions in a patient currently fall into one of three categories:

- A relatively simple analytical calculation of first order Compton scatter and its addition to the primary dose at the point of interest. The method is fairly rudimentary as it assumes a parallel beam of monoenergetic photons and ignores heterogeneities and scattering higher than of the first order.
- The convolution–superposition method, which accounts for the indirect nature of dose deposition from photon interactions, separating the primary photon interactions from the transport of scattered photons and charged particles produced through the photoelectric effect (photoeffect), Compton scattering and pair production.

- The Monte Carlo method, which is the most promising of the model based dose computation methods, uses well established probability distributions governing the individual interactions of photons and electrons with the patient and their transport through the patient. Monte Carlo simulation is essential in all model based dose computations to characterize the clinical beam emanating from the radiation source, but can also be used directly to compute photon dose distributions for a given patient and treatment geometry. The current limitation of direct Monte Carlo calculations is the time required to calculate the large number of histories required to reduce stochastic or random uncertainties to acceptable levels. It is expected that advances in computer technology will, within a few years, reduce Monte Carlo calculation times to acceptable levels, and this will make Monte Carlo methods the standard approach to radiotherapy treatment planning. The electron densities for various tissues of individual patients are obtained with CT scanners or CT simulators and form an essential component of any Monte Carlo based dose distribution calculation.

6.12. CLARKSON SEGMENTAL INTEGRATION

Tables for the various dose functions, such as the PDD, TAR, PSF and TMR, etc., are usually given for a series of square fields. Values for these functions when fields are rectangular or circular may be obtained through determining the equivalent square for the rectangular field (Eq. (6.25)) or circular field (Eq. (6.26)) and then using the appropriate tabulated square field data for determining the value of a given dose function. Here, an assumption is made that there is a match between dose functions for rectangular fields and their equivalent square and circular fields. It has been shown experimentally that this assumption is valid for the range of field sizes and beam energies used in radiotherapy.

Radiation fields other than square, rectangular or circular are termed irregular fields. An irregular field will also have an equivalent square field and an equivalent circular field that will yield the same value of a given dose function as does the irregular field, but there are no simple means to determine the equivalent square or circle for a given irregular field. However, a technique, referred to as the Clarkson segmental integration, can be used to calculate the appropriate value of any given dose function for the given irregular field based on circular field data.

The Clarkson technique resolves the irregular field into sectors of circular beams originating at the point of interest Q in the phantom or patient. For

manual calculations, sectors with an angular width of 10º are usually used; for computer driven calculations the angular width is 5º or even smaller, in order to improve accuracy.

An assumption is made that a sector with a given field radius contributes $1/N$ of the total circular field value to the value of the given function F for the irregular field at point Q, where N is the number of sectors in a full circle of 360º.

The value of a given function F for an irregular field that in general depends on depth z of point Q, shape of the irregular field, SSD = f and beam energy $h\nu$ is then determined from the following segmental integration relationship:

$$F(z, \text{ irregular field}, f, h\nu) = \frac{1}{N}\sum_{i=1}^{N} F(z, r_i, f, h\nu) \tag{6.68}$$

where

N is the number of sectors in 360º (for manual calculations $N = 36$);

r_i is the radius from point Q to the edge of the field at the centre of sector i;

$F(z, r_i, f, h\nu)$ is the value of the dosimetric function F at depth z, SSD = f and beam energy $h\nu$ for the circular field with radius r_i.

An example of an irregular field is shown in Fig. 6.20 with two of 36 sectors highlighted: one is a simple sector with radius r_1 and the other is a composite sector with three radii: r_a, r_b and r_c.

- The contribution of the simple sector to the sum in Eq. (6.68) is simply equal to:

  $(1/N)F(z, r_i, f, h\nu)$

- The composite sector consists of three components to yield the following contribution:

  $(1/N)[F(z, r_a, f, h\nu) - F(z, r_b, f, h\nu) + F(z, r_c, f, h\nu)]$

  to the sum given in Eq. (6.68), with two positive components that are contributed by portions of the radiation field and one negative

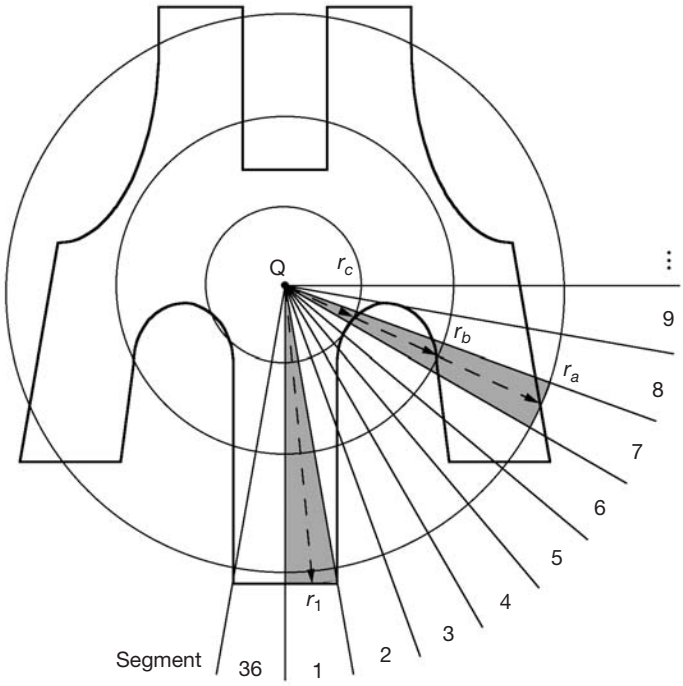

FIG. 6.20. An example of a mantle irregular field. Two segments out of 36 are highlighted. The first is simple with radius r_1, the seventh is composite with three radii: r_a, r_b and r_c.

component that accounts for the missing portion of the radiation field in the segment (sector).

Once the value of a dose function for a given irregular field is determined through the Clarkson integration technique, the equivalent square for the irregular field is also established by finding in tabulated square field data the square field that will give the same value for the dose function. The segmental integration technique was originally proposed by Clarkson in the 1940s and developed by Johns and Cunningham in the 1960s for determining the scatter component of the dose at an arbitrary point of interest in the patient, either inside or outside the direct radiation field.

For points inside the radiation field the scatter component is added to the primary beam component; for points outside the field the scatter component is added to the radiation transmitted through the shielding blocks, collimator or head shielding of the treatment machine.

The original implementation of the Clarkson technique was intended for use with orthovoltage and cobalt beams for which the primary dose rate was reasonably flat from the central axis to points near the edge of the field, where it began to decrease. In linac beams, however, the primary dose rate at shallow depths in the patient may actually increase at distances away from the central axis ('horns') as a result of flattening filter effects on the radiation beam. A flattening filter correction that depends on depth z in a phantom and radial distance r from the central axis is required to model, for the primary beam component, this increase in the dose rate away from the central beam axis.

6.13. RELATIVE DOSE MEASUREMENTS WITH IONIZATION CHAMBERS

Ionization chambers are used in clinical physics not only for photon and electron beam calibration at a reference point in a phantom but also for relative measurements of various parameters and dose functions, such as the CF, the RDF, dose profiles and PDDs, including the surface dose and doses in the buildup region. The dependence of various dose correction factors (such as ionization chamber polarity, ionic recombination, stopping power ratios and fluence correction) on beam energy (i.e. depth in a phantom) should be considered in relative dose measurements, although in many situations the dependence may be ignored.

Usually each task of dose determination is carried out with ionization chambers designed for the specific task at hand. For example:

- Doses and dose rates at reference points in a phantom for megavoltage photon beams and electron beams above 10 MeV are measured with relatively large volume (0.6 cm^3) cylindrical ionization chambers in order to obtain a reasonable signal and good signal to noise ratio.
- Relative dose distributions (e.g. central axis PDDs and beam profiles) for photon beams beyond z_{max} and for electron beams are usually measured with small volume (0.1 cm^3) ionization chambers in order to obtain good spatial resolution.
- Surface doses and doses in the buildup region for photon beams are measured with parallel-plate ionization chambers incorporating a thin polarizing electrode window (to be able to measure the surface dose) and a small electrode separation (typically 1 mm, for better spatial resolution).

- A typical megavoltage photon beam PDD curve, measured with positive and negative polarities with a parallel-plate ionization chamber in the dose buildup region and beyond, is shown in Fig. 6.21.
- In the buildup region the positive chamber polarity produces a larger signal than the negative polarity. The difference in signals is most pronounced on the phantom surface and then diminishes with depth until it disappears at depths of z_{max} and beyond. At z_{max} and beyond this curve is more conveniently measured with small volume cylindrical ionization chamber; the results will match those obtained with a parallel-plate chamber. In the buildup region, however, the cylindrical chamber will read an unrealistically high signal because of its excessive wall thickness.
- In the buildup region, signals for both positive and negative chamber polarities are measured with a parallel-plate ionization chamber, and the average reading between the two polarities is used as the true dose value. Signal averaging eliminates the chamber Compton current that results from photon interactions in the measuring electrode of the chamber. In the dose buildup region, these interactions cause a loss of electrons from the measuring electrode that is not fully compensated by the arrival of

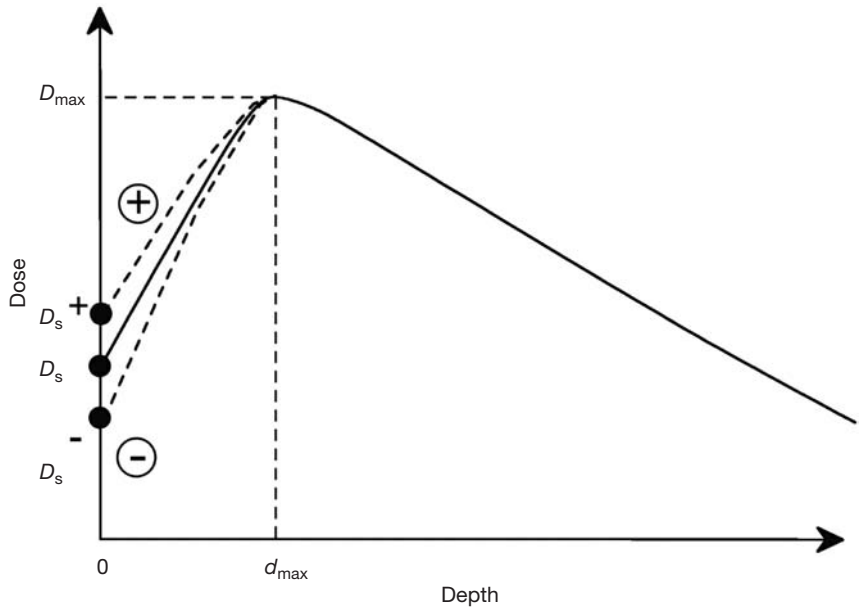

FIG. 6.21. Megavoltage photon beam depth doses measured with a parallel-plate ionization chamber. In the buildup region the positive polarity produces a higher reading than the negative polarity, beyond z_{max} both polarities give essentially identical signals.

electrons from the upper layers of the phantom. The electron difference results in a non-dosimetric current, which is referred to as the Compton current, and causes an increased reading for positive chamber polarity and a decreased reading for negative chamber polarity.

- For depths beyond z_{max}, both positive and negative chamber polarities yield the same reading, because electronic equilibrium exists on the measuring electrode (as many electrons land on the measuring electrode as are ejected by photon interactions from the measuring electrode).
- Ionic collection efficiency depends not only on the potential difference between the polarizing and measuring electrodes but also on the dose rate in the ionization chamber cavity. Therefore, in principle, when measuring depth doses, one should account for the change in ionic collection efficiency as a function of depth in a phantom. However, in practice, since ionic recombination loss in well behaved chambers is 2% or less, the changes in ionic recombination with depth are ignored when measuring relative depth doses.
- In general, stopping power ratios water to air and chamber correction factors are also depth dependent, and this dependence, according to the particular situation and accuracy required, might have to be accounted for when measuring depth doses with ionization chambers:
  - In photon beams, since the restricted stopping power ratio water to air is essentially independent of depth at depths larger than z_{max}, the signal corrected for the polarity effect can be treated as an indication of the relative dose to water. At depths shallower than z_{max}, the restricted stopping power ratio water to air varies by up to 2%, depending on field size and energy, a variation that is usually ignored.
  - In electron beams, the restricted stopping power ratio water to air varies significantly as a function of depth, requiring a correction to the measured ionization curve when relative dose is to be determined. For realistic beams as a function of depth z and energy (parametrized by R_{50}) the stopping power ratio water to air is given by the following fit (Burns et al.):

$$\left(\frac{\overline{L}}{\rho}\right)_{\text{air}}^{\text{water}}(z, R_{50}) = \frac{a + b(\ln R_{50}) + c(\ln R_{50})^2 + d(z/R_{50})}{1 + e(\ln R_{50}) + f(\ln R_{50})^2 + g(\ln R_{50})^3 + h(z/R_{50})} \tag{6.69}$$

with the following values for the parameters: $a = 1.0752$; $b = -0.50867$; $c = 0.088670$; $d = -0.08402$; $e = -0.42806$; $f = 0.064627$; $g = 0.003085$; and $h = -0.12460$.

- Finally, in electron beams, for unguarded chambers (such as Farmer type thimble chambers), the fluence perturbation correction factor also varies as a function of energy at depth (by up to 5% in the range between z_{max} and the bremsstrahlung tail for a 20 MeV electron beam). Well guarded parallel-plate ionization chambers are therefore better suited for measurement of relative depth doses in electron beams than are thimble chambers.

6.14. DELIVERY OF DOSE WITH A SINGLE EXTERNAL BEAM

Outputs for X ray machines and isotope units are usually given in centigray per minute (cGy/min) at z_{max} in a phantom, while outputs for linacs are given in centigray per monitor unit (cGy/MU) at z_{max} in a phantom.

Transmission ionization chambers in linacs are usually adjusted such that the beam output corresponds to 1 cGy/MU at z_{max} for a 10×10 cm^2 field at SSD = 100 cm (i.e. $\dot{D}_P(z_{max}, 10, 100, h\nu) = 1$ cGy/MU (Fig. 6.9)).

$\dot{D}_P(z_{max}, A, 100, h\nu)$, the dose rate at point P for an arbitrary field size A, is then obtained from $\dot{D}_P(z_{max}, 10, 100, h\nu)$ as follows (see Eq. (6.30)):

$$\dot{D}_P(z_{max}, A, 100, h\nu) = \dot{D}_P(z_{max}, 10, 100, h\nu) \times \mathrm{RDF}(A, h\nu) \tag{6.70}$$

The number of monitor units $\mathcal{MU}$ (in MUs) required to deliver a tumour dose TD at point Q (Fig. 6.9) using a single SSD field with field A is calculated from Eq. (6.34) recognizing that $\dot{D}_Q = \mathrm{T\dot{D}} = (\mathrm{TD})/(\mathcal{MU})$, where $\mathrm{T\dot{D}}$ is the tumour dose rate:

$$\mathcal{MU} = \frac{\mathrm{TD}}{\dot{D}_P(z_{max}, 10, 100, h\nu) \times \mathrm{RDF}(A, h\nu) \times \mathrm{PDD}(z, A, f, h\nu)} \tag{6.71}$$

Similarly, for an SAD set-up (Fig. 6.15) the number of monitor units $\mathcal{MU}$ to deliver a tumour dose TD at point Q with a single isocentric beam with field size A_Q may be calculated using Eq. (6.52) recognizing that $\dot{D}_Q = \mathrm{T\dot{D}} = (\mathrm{TD})/(\mathcal{MU})$ and that $\dot{D}_{Qmax}(z_{max}, A_Q, \mathrm{SAD} = 100, h\nu)$ may be approximated as:

$$\dot{D}_{\mathrm{Qmax}}(z_{\max}, A_{\mathrm{Q}}, 100_{\mathrm{SAD}}, h\nu)$$
$$\approx \dot{D}_{\mathrm{P}}(z_{\max}, 10, 100_{\mathrm{SSD}}, h\nu) \times \mathrm{RDF}(A, h\nu) \times \left(\frac{f + z_{\mathrm{ref}}}{f}\right)^2 \qquad (6.72)$$

to obtain:

$$\mathcal{MU} = \frac{\mathrm{TD}}{\dot{D}_{\mathrm{P}}(z_{\max}, 10, 100_{\mathrm{SSD}}, h\nu) \times \mathrm{RDF}(A, h\nu) \times \mathrm{TPR}(z, A_{\mathrm{Q}}, h\nu) \times \left(\frac{f}{f + z_{\mathrm{ref}}}\right)^2} \qquad (6.73)$$

6.15. EXAMPLE OF DOSE CALCULATION

Given $\dot{D}(15, 15, 80, \mathrm{Co})$ calculate $\dot{D}(10, 20, 140, \mathrm{Co})$, where $\dot{D}(15, 15, 80, \mathrm{Co}) = \dot{D}(z, A, f, \mathrm{Co})$ stands for the dose rate in cGy/min at point Q in a water phantom at a depth $z = 15$ cm on the central axis of a cobalt beam with a field size $A = 15 \times 15$ cm^2 and $SSD = f = 80$ cm.

The problem ties together the various basic functions and parameters that are routinely used in external beam radiotherapy and may be solved using either the SSD approach (with PDDs) or the SAD approach (with TARs). The two approaches, of course, should yield the same end result. The steps involved in going from $\dot{D}(15, 15, 80, \mathrm{Co})$ to $\dot{D}(10, 20, 140, \mathrm{Co})$ are given below for the SSD and the SAD approaches.

SSD approach (6.74)	SAD approach (6.75)
$\dot{D}(15,15,80,\mathrm{Co})$	$\dot{D}(15,15,80,\mathrm{Co})$
$\downarrow \quad \times \dfrac{100}{\mathrm{PDD}(15,15,80,\mathrm{Co})}$	$\downarrow \quad \times \dfrac{1}{\mathrm{TAR}(15,17.8,\mathrm{Co})}$
$\dot{D}(0.5,15,80,\mathrm{Co})$	$\dot{D}'_{95}(17.8,\mathrm{Co})$
$\downarrow \quad \times \dfrac{1}{\mathrm{PSF}(15,\mathrm{Co})}$	$\downarrow \quad \times \dfrac{95^2}{80.5^2}$

$$\dot{D}'_{80.5}(15_{80}, \mathrm{Co}) \qquad \dot{D}'_{80.5}(15_{80}, \mathrm{Co})$$

$$\downarrow \quad \times \frac{\mathrm{CF}(11.4,\mathrm{Co})}{\mathrm{CF}(15,\mathrm{Co})} \qquad \downarrow \quad \times \frac{\mathrm{CF}(11.4,\mathrm{Co})}{\mathrm{CF}(15,\mathrm{Co})}$$

$$\dot{D}'_{80.5}(11.4_{80},\mathrm{Co}) \qquad \dot{D}'_{80.5}(11.4_{80},\mathrm{Co})$$

$$\downarrow \quad \times \frac{80.5^2}{140.5^2} \qquad \downarrow \quad \times \frac{80.5^2}{150^2}$$

$$\dot{D}'_{140.5}(20_{140},\mathrm{Co}) \qquad \dot{D}'_{150}(21.4_{150},\mathrm{Co})$$

$$\downarrow \quad \times \mathrm{PSF}(20,\mathrm{Co}) \qquad \downarrow \quad \times \mathrm{TAR}(10,21.4,\mathrm{Co})$$

$$\dot{D}(0.5,20,140,\mathrm{Co}) \qquad \dot{D}(10,20,140,\mathrm{Co})$$

$$\downarrow \quad \times \mathrm{PDD}(10,20,140,\mathrm{Co})/100$$

$$\dot{D}(10,20,140,\mathrm{Co})$$

where $\dot{D}'_{140.5}(20_{140},\mathrm{Co})$ stands for the 'dose rate to small mass of water' at a distance of 140.5 cm from the source with the collimator set to give 20×20 cm^2 at 140 cm from the source, corresponding to 11.4×11.4 cm^2 at 80 cm from the source.

The general answer for the SSD approach is:

$$\frac{\dot{D}(10,20,140,\mathrm{Co})}{\dot{D}(15,15,80,\mathrm{Co})}$$

$$= \frac{\mathrm{PDD}(10,20,140,\mathrm{Co})}{\mathrm{PDD}(15,15,80,\mathrm{Co})} \times \frac{\mathrm{PSF}(20,\mathrm{Co})}{\mathrm{PSF}(15,\mathrm{Co})} \times \frac{\mathrm{CF}(11.4,\mathrm{Co})}{\mathrm{CF}(15,\mathrm{Co})} \times \frac{80.5^2}{140.5^2}$$

$$= \frac{\mathrm{PDD}(10,20,140,\mathrm{Co})}{\mathrm{PDD}(15,15,80,\mathrm{Co})} \times \frac{\mathrm{RDF}(20,\mathrm{Co})}{\mathrm{RDF}(15,\mathrm{Co})} \times \frac{\mathrm{CF}(11.4,\mathrm{Co})}{\mathrm{CF}(20,\mathrm{Co})} \times \frac{80.5^2}{140.5^2} \tag{6.76}$$

The general answer for the SAD approach is:

$$\frac{\dot{D}(10,20,140,\mathrm{Co})}{\dot{D}(15,15,80,\mathrm{Co})} = \frac{\mathrm{TAR}(10,21.4,\mathrm{Co})}{\mathrm{TAR}(15,17.8,\mathrm{Co})} \times \frac{\mathrm{CF}(11.4,\mathrm{Co})}{\mathrm{CF}(15,\mathrm{Co})} \times \frac{95^2}{150^2} \tag{6.77}$$

Both answers with standard ^{60}Co machine data (see, for example, Br. J. Radiol. Suppl. 25) will yield for the ratio of the two dose rates 0.505 within ±1%.

In Eq. (6.74) we go to $\dot{D}'_{80.5}(11.4,\mathrm{Co})$ from $\dot{D}(0.5,15,80,\mathrm{Co})$ following a path that leads through $\dot{D}'_{80.5}(15_{80},\mathrm{Co})$ as follows:

$$\dot{D}'_{80.5}(11.4,\mathrm{Co}) = \dot{D}(0.5,15,80,\mathrm{Co}) \times \frac{1}{\mathrm{PSF}(15,\mathrm{Co})} \times \frac{\mathrm{CF}(11.4,\mathrm{Co})}{\mathrm{CF}(15,\mathrm{Co})} \tag{6.78}$$

We can also attain $\dot{D}'_{80.5}(11.4,\mathrm{Co})$ by going in a phantom from $\dot{D}(0.5,15,80,\mathrm{Co})$ to $\dot{D}(0.5,11.4,80,\mathrm{Co})$ and then to $\dot{D}'_{80.5}(11.4_{80},\mathrm{Co})$ as follows:

$$\begin{aligned}
&\dot{D}(0.5,15,80,\mathrm{Co}) \\
&\downarrow \quad \times \frac{\mathrm{RDF}(11.4,\mathrm{Co})}{\mathrm{RDF}(15,\mathrm{Co})} \\
&\dot{D}(0.5,11.4,80,\mathrm{Co}) \\
&\downarrow \quad \times \frac{1}{\mathrm{PSF}(11.4,\mathrm{Co})} \\
&\dot{D}'_{80.5}(11.4_{80},\mathrm{Co})
\end{aligned} \tag{6.79}$$

Both paths, of course, will give identical end results, since, as can be shown using Eqs (6.29) and (6.31):

$$\frac{1}{\mathrm{PSF}(15,\mathrm{Co})} \times \frac{\mathrm{CF}(11.4,\mathrm{Co})}{\mathrm{CF}(15,\mathrm{Co})} = \frac{\mathrm{RDF}(11.4,\mathrm{Co})}{\mathrm{RDF}(15,\mathrm{Co})} \times \frac{1}{\mathrm{PSF}(11.4,\mathrm{Co})} \tag{6.80}$$

6.16. SHUTTER CORRECTION TIME

In radiotherapy machines that use an electrical timer for measuring the dose delivery (radiotherapy X ray machines and teletherapy radioisotope machines), account must be taken of possible end effects (shutter correction

time) resulting from switching the beam on and off. In X ray machines the beam output builds up from zero to its full value as the generating voltage builds up in the first few seconds of the treatment. In isotope machines the source is moved into position at the start of the treatment and is returned to its safe position at the end of the treatment.

The shutter correction time τ_s is defined as the time that must be added to or subtracted from the calculated treatment time T_c to deliver accurately the prescribed dose to the patient. For a given therapy machine the shutter correction time is typically determined by measuring two doses (D_1 and D_n) at a given point P (e.g. at z_{max} in a phantom):

- D_1 is measured with a relatively long exposure time T (of the order of 5 min), contains one end effect and is given by $D_1 = \dot{D}(T + \tau_s)$ or $\dot{D} = D_1/(T + \tau_s)$.
- D_n is measured cumulatively with n dose segments, each having an exposure time T/n. The dose D_n thus contains n end effects; the cumulative beam-on time is again equal to T, and D_n is given by $D_n = \dot{D}(T + n\tau_s)$ or $\dot{D} = D_n/(T + n\tau_s)$.

Solving the equation for the true dose rate $\dot{D} = D_1/(T+\tau_s) = D_n/(T + n\tau_s)$ for the shutter correction time τ_s gives:

$$\tau_s = (D_n - D_1)T/(nD_1 - D_n) \tag{6.81}$$

In Eq. (6.81) $\tau_s > 0$ for $D_n > D_1$; $\tau_s = 0$ for $D_n = D_1$; and $\tau_s < 0$ for $D_n < D_1$. The time set on the timer will be $(T_c - \tau_s)$. Typical shutter correction times are of the order of 1 s.

BIBLIOGRAPHY

BRITISH JOURNAL OF RADIOLOGY, Central Axis Depth Dose Data for Use in Radiotherapy, Suppl. 25 (1996).

BURNS, D.T., DING, G.X., ROGERS, D.W.O., R_{50} as beam quality specifier for selecting stopping power ratios and reference depths for electrons, Med. Phys. **23** (1996) 383–388.

HENDEE, W.R., IBBOTT, G.S., Radiation Therapy Physics, Mosby, St. Louis, MI (1996).

JOHNS, H.E., CUNNINGHAM, J.R., The Physics of Radiology, Thomas, Springfield, IL (1984).

KHAN, F.M., The Physics of Radiation Therapy, Lippincott, Williams and Wilkins, Baltimore, MD (2003).

WILLIAMS, J.R., THWAITES, D.I. (Eds), Radiotherapy Physics in Practice, Oxford University Press, Oxford (2000).